Thermodynamic Casimir force: A Monte Carlo study of the crossover between the ordinary and the normal surface universality class

Martin Hasenbusch*

Institut für Physik, Humboldt-Universität zu Berlin, Newtonstrasse 15, D-12489 Berlin, Germany

(Received 7 January 2011; published 20 April 2011)

We study the crossover from the ordinary to the normal surface universality class in the three-dimensional Ising bulk universality class. This crossover is relevant for the behavior of films of binary mixtures near the demixing point and a weak adsorption at one or both surfaces. We perform Monte Carlo simulations of the improved Blume-Capel model on the simple cubic lattice. We consider systems with film geometry, where various boundary conditions are applied. We discuss corrections to scaling that are caused by the surfaces and their relation with the so called extrapolation length. To this end, we analyze the behavior of the magnetization profile near the surfaces of films. We obtain an accurate estimate of the renormalization-group exponent $y_{h_1} = 0.7249(6)$ for the ordinary surface universality class. Next we study the thermodynamic Casimir force in the crossover region from the ordinary to the normal surface universality class. To this end, we compute the Taylor expansion of the crossover finite-size scaling function up to the second order in h_1 around $h_1 = 0$, where h_1 is the external field at one of the surfaces. We check the range of applicability of the Taylor expansion by simulating at finite values of h_1. Finally, we study the approach to the strong adsorption limit $h_1 \to \infty$. Our results confirm the qualitative picture that emerges from exact calculations for stripes of the two-dimensional Ising model [D. B. Abraham and A. Maciołek, Phys. Rev. Lett. **105**, 055701 (2010)], mean-field calculations, and preliminary Monte Carlo simulations of the Ising model on the simple cubic lattice [T. F. Mohry *et al.*, Phys. Rev. E **81**, 061117 (2010)]: For certain choices of h_1 and the thickness of the film, the thermodynamic Casimir force changes sign as a function of the temperature, and for certain choices of the temperature and h_1, it also changes sign as a function of the thickness of the film.

DOI: 10.1103/PhysRevB.83.134425 PACS number(s): 05.50.+q, 05.70.Jk, 05.10.Ln, 68.15.+e

I. INTRODUCTION

In 1978, Fisher and de Gennes[1] realized that when thermal fluctuations are restricted by a container, a force acts on its walls. Since this effect is analogous to the Casimir effect,[2] where the restriction of quantum fluctuations induces a force, it is called the "thermodynamic" Casimir effect. Since thermal fluctuations only extend to large scales in the neighborhood of continuous phase transitions, it is also called the "critical" Casimir effect. Recently, this force could be detected for various experimental systems, and quantitative predictions could be obtained from Monte Carlo simulations of spin models.[3]

The behavior of the thermodynamic Casimir force can be described by finite-size scaling (FSS)[4] laws. For the film geometry that we consider here, one gets[5] for the thermodynamic Casimir force per area

$$F_{\text{Casimir}} \simeq k_B T L_0^{-3}\, \theta_{(\text{UC}_1,\text{UC}_2)}(t[L_0/\xi_0]^{1/\nu}), \qquad (1)$$

where L_0 is the thickness of the film, $t = (T - T_c)/T_c$ is the reduced temperature, and T_c is the critical temperature. Note that below, analyzing our data, we shall use for simplicity the definition $t = \beta_c - \beta$, where $\beta = 1/k_B T$. The amplitude ξ_0 of the correlation length ξ is defined by

$$\xi = \xi_{0,\pm}|t|^{-\nu} \times (1 + a_\pm |t|^{\nu\omega} + ct + \cdots), \qquad (2)$$

where $-$ and $+$ indicate the high- and the low-temperature phase, respectively. Since the correlation length can be determined more accurately in the high-temperature phase than in the low-temperature phase, we take $\xi_0 = \xi_{0,+}$ in Eq. (1). The power law (2) is subject to confluent corrections such as $a_\pm |t|^{\nu\omega}$, and nonconfluent ones such as ct. Critical exponents such as ν and ratios of amplitudes such as $\xi_{0,+}/\xi_{0,-}$ are universal. Also, correction exponents such as ω and ratios of correction amplitudes such as a_+/a_- are universal. For the three-dimensional Ising universality class considered here, $\nu\omega \approx 0.5$. For reviews on critical phenomena and their modern theory, i.e., the renormalization group (RG), see, e.g., Refs. 6–9. The universal finite-size scaling function $\theta_{(\text{UC}_1,\text{UC}_2)}$ depends on the universality class of the bulk system as well as the surface universality classes UC_1 and UC_2 of the two surfaces of the film. For reviews on surface critical phenomena, see, e.g., Refs. 10–12. We shall give a brief discussion below in Sec. III.

In the past few years, there has been great interest in the crossover behaviors of the thermodynamic Casimir force. In Ref. 13, the authors studied the crossover from the special surface universality class to the ordinary one by using field theoretic methods. They found that for certain choices of the parameters, the thermodynamic Casimir force changes sign with a varying thickness of the film. The authors of Ref. 14 computed exactly the thermodynamic Casimir force for stripes of the two-dimensional Ising model as a function of the external surface fields h_1 and h_2. Also here the authors found that for certain choices of the fields h_1 and h_2, the thermodynamic Casimir force does change sign as a function of the temperature or the thickness of the film. More recently, the authors of Ref. 15 studied the crossover from the ordinary to the normal surface universality class, and the crossover from the special to the ordinary as well as the normal surface universality class using the mean-field approximation. Also in these cases, a change of sign of the thermodynamic Casimir

force could be observed. Furthermore, in Ref. 15, preliminary results[16] of Monte Carlo simulations of the spin-1/2 Ising model on the simple cubic lattice for the crossover from the ordinary to the normal surface universality class were presented. Following the authors of Ref. 15, these observations might be of technological relevance. They write, "Such a tunability of critical Casimir forces toward repulsion might be relevant for micro- and nano-electromechanical systems in order to prevent stiction due to the omnipresent attractive quantum mechanical Casimir forces.[2,17]" In recent experiments on colloidal particles immersed in a binary mixture of fluids,[18] the authors demonstrated that the adsorption strength can be varied continuously by a chemical modification of the surfaces. In particular, the situation of effectively equal adsorption strengths for the two fluids can be reached. For sufficiently small ordering interaction at the surface, this corresponds to the ordinary surface universality class. Hence these experiments open the way to study the crossover from the ordinary to the normal universality class. As discussed in Refs. 19–22, effectively weak adsorption can also be obtained by using patterned substrates.

In the present work, we compute scaling functions for the film or plate-plate geometry. To compare with experiments on the thermodynamic Casimir force between colloidal particles and a flat substrate as studied in Ref. 18, the scaling function for the plate-sphere geometry has to be computed. The Derjaguin approximation[23] might be used to derive scaling functions for the plate-sphere geometry from those for the plate-plate geometry if the radius of the sphere is large compared with the distance between the plate and the sphere,[24,25] as is indeed the case in Ref. 18. In recent works,[26,27] the Derjaguin approximation had been used to obtain the scaling functions for the plate-sphere geometry in the strong adsorption limit starting from the Monte Carlo estimates of Refs. 28 and 29 for the film geometry.

As in Ref. 30, where we had studied the strong adsorption limit, we shall study the crossover by performing Monte Carlo simulations of the improved Blume-Capel model on the simple cubic lattice. We shall give the definition of this model in Sec. II below. "Improved" means that corrections to finite-size scaling that are $\propto L_0^{-\omega}$ vanish. This property is very useful in the study of films, since typically the surfaces cause corrections $\propto L_0^{-1}$,[10–12] and when fitting Monte Carlo data it is quite difficult to disentangle corrections that have similar exponents. Motivated by the experiments of Ref. 18, we shall mainly study films where the external field h_1 at the first surface is finite, while at the other surface the limit $h_2 \to \infty$ is taken, corresponding to the strong adsorption limit in a binary mixture. For this choice of boundary conditions, the correlation length of the film divided by its thickness remains small at any temperature. In contrast, for $h_1 = h_2 = 0$ the film undergoes a second-order phase transition in the universality class of the two-dimensional Ising model. This implies that in the neighborhood of this transition, the correlation length of the film divided by its thickness is large. Therefore, the Monte Carlo study of the crossover from $h_1 = h_2 = 0$ to the limit $|h_1|,|h_2| \to \infty$ would be more involved than that performed here.

In preparation for our study of the thermodynamic Casimir force, we have accurately determined the surface critical exponent y_{h_1} of the ordinary surface universality class. Furthermore, we have estimated the so called extrapolation length for various boundary conditions. The extrapolation length is directly related to the corrections to finite-size scaling that are caused by the surfaces of the film. Our numerical results are mainly based on the analysis of the behavior of the magnetization profile at the bulk critical temperature. Next, we computed the thermodynamic Casimir force for the range of inverse temperatures around the bulk critical point where, at the level of our numerical accuracy, it is nonvanishing. To this end we follow the suggestion of Hucht.[31] For alternative methods, see Refs. 28,29,32 and 33. Note that the stress tensor method of Ref. 34 can only be applied for periodic or antiperiodic boundary conditions. First we have simulated films with a vanishing surface field $h_1 = 0$. Based on the data obtained from these simulations, we have also computed the Taylor expansion of the thermodynamic Casimir force per area in h_1 up to second order around $h_1 = 0$. We demonstrate that, taking into account corrections $\propto L_0^{-1}$, already for the relatively small thicknesses $L_0 = 8.5$, 12.5, and 16.5 the behavior of the thermodynamic Casimir force per area as well as its partial derivatives with respect to h_1 are well described by universal FSS functions. Next, we simulated films with various finite values of h_1 to check the range of applicability of the Taylor expansion and to study the crossover beyond this range. Finally, we studied the approach to the strong adsorption limit $h_1 \to \infty$. Qualitatively, we confirm the picture that emerges from the exact solution of the two-dimensional Ising model[14] and the mean-field calculation.[15]

The outline of the paper is the following: In Sec. II, we define the model and the observables that we have studied. In Sec. III, we briefly review the phase diagram of a semi-infinite system. Then in Sec. IV, we discuss the finite-size scaling behavior of the magnetization profile at the bulk critical point and the finite-size scaling behavior of the thermodynamic Casimir force. In Sec. V, we discuss how to compute the thermodynamic Casimir force and its partial derivatives with respect to the external field h_1 at the surface. In Sec. VI, we present the results of our Monte Carlo simulations. We performed a series of simulations at the bulk critical point, where we focused on the magnetization profile. Next, we determined the thermodynamic Casimir force per area in the neighborhood of the bulk critical point for various values of the external field h_1 at the surface. Finally, in Sec. VII, we summarize and conclude.

II. THE MODEL AND BULK OBSERVABLES

We study the Blume-Capel model on the simple cubic lattice. It is characterized by the reduced Hamiltonian

$$H = -\beta \sum_{\langle xy \rangle} s_x s_y + D \sum_x s_x^2 - h \sum_x s_x, \qquad (3)$$

where $x = (x_0,x_1,x_2)$ denotes a site of the lattice. The components x_0, x_1, and x_2 take integer values. The spin s_x might take the values -1, 0, or 1. In the following, we shall consider a vanishing external field $h = 0$ throughout. The parameter D controls the density of vacancies $s_x = 0$. In the limit $D \to -\infty$, the spin-1/2 Ising model is recovered. For $-\infty \leqslant D < D_{\rm tri}$, the model undergoes a second-order

phase transition in the three-dimensional Ising universality class. For $D > D_{\rm tri}$, the transition is of first order. The most recent estimate for the tricritical point is $D_{\rm tri} = 2.0313(4)$.[35] Numerically, using Monte Carlo simulations it has been shown that there is a point $(D^*,\beta_c(D^*))$ on the line of second-order phase transitions where the amplitude of leading corrections to scaling vanishes. Our most recent estimate is $D^* = 0.656(20)$.[36] In Ref. 36, we have simulated the model at $D = 0.655$ close to β_c on lattices of a linear size up to $L = 360$. From a standard finite-size scaling analysis of phenomenological couplings such as the Binder cumulant, we find

$$\beta_c(0.655) = 0.387\,721\,735(25) \tag{4}$$

for the inverse of the critical temperature at $D = 0.655$. The amplitude of leading corrections to scaling at $D = 0.655$ is at least a factor of 30 smaller than for the spin-1/2 Ising model.

Our recent estimates for bulk critical exponents in the three-dimensional Ising universality class are[36]

$$\nu = 0.630\,02(10), \tag{5}$$

$$\eta = 0.036\,27(10), \tag{6}$$

$$\omega = 0.832(6). \tag{7}$$

In the following, we set the scale by using the second moment correlation length $\xi_{\rm 2nd}$ in the high-temperature phase of the model. On a finite lattice of the linear size L in each of the directions, it might be defined by

$$\xi_{\rm 2nd} = \sqrt{\frac{\chi/F - 1}{4\sin^2 \pi/L}}, \tag{8}$$

where

$$F = \frac{1}{L^3}\left\langle \left| \sum_x \exp\left(i\frac{2\pi x_k}{L}\right) s_x \right|^2 \right\rangle \tag{9}$$

is the Fourier transform of the correlation function at the lowest nonzero momentum, and

$$\chi = \frac{1}{L^3}\left\langle \left(\sum_x s_x \right)^2 \right\rangle \tag{10}$$

is the magnetic susceptibility. In Refs. 30 and 37, we find

$$\begin{aligned}\xi_{\rm 2nd,0,+} &= 0.2282(2) - 1.8 \times (\nu - 0.630\,02) \\ &\quad + 250 \times (\beta_c - 0.387\,721\,735)\end{aligned} \tag{11}$$

for the amplitude of the second moment correlation length in the high-temperature phase, where we have used

$$t = \beta_c - \beta \tag{12}$$

as a definition of the reduced temperature. We shall use this definition of t also in the following. The energy density is defined by

$$E_{\rm bulk} = \frac{1}{L^3}\sum_{\langle xy\rangle}\langle s_x s_y\rangle. \tag{13}$$

In the following, we shall need the energy density of the bulk system in a neighborhood of the bulk critical point. To this end, we have performed simulations at 350 different values of β in the range $0.25 \leqslant \beta \leqslant 0.6$.[37] In a small neighborhood of β_c, where no direct simulations are available, we use

$$\begin{aligned}E_{\rm bulk}(\beta) &= E_{ns} + C_{ns}(\beta - \beta_c) + a_\pm|\beta - \beta_c|^{1-\alpha} \\ &\quad + d_{ns}(\beta - \beta_c)^2 + b_\pm|\beta - \beta_c|^{2-\alpha}.\end{aligned} \tag{14}$$

For a discussion, see Sec. IV of Ref. 37.

A. Film geometry and boundary conditions

Here we study systems with a film geometry. In the ideal case, this means that the system has a finite thickness L_0, while in the other two directions the thermodynamic limit $L_1, L_2 \to \infty$ is taken. In our Monte Carlo simulations, we shall study lattices with $L_0 \ll L_1 = L_2 = L$ and apply periodic boundary conditions in the 1 and 2 directions.

The reduced Hamiltonian of the Blume-Capel model with film geometry is

$$\begin{aligned}H = &-\beta\sum_{\langle xy\rangle} s_x s_y + D\sum_x s_x^2 \\ &- \beta_1 \sum_{\langle xy\rangle, x_0=y_0=1} s_x s_y \; - \; \beta_2 \sum_{\langle xy\rangle, x_0=y_0=L_0} s_x s_y \\ &- h_1 \sum_{x, x_0=1} s_x \; - \; h_2 \sum_{x, x_0=L_0} s_x,\end{aligned} \tag{15}$$

where $h_1, h_2 \neq 0$ break the symmetry at the surfaces that are located at $x_0 = 1$ and $x_0 = L_0$, respectively. In our convention, $\langle xy\rangle$ runs over all pairs of nearest-neighbor sites with fluctuating spins. Note that here the sites $(1,x_1,x_2)$ and (L_0,x_1,x_2) are not nearest neighbors, as would be the case for periodic boundary conditions. In our study, we set $\beta_1 = \beta_2 = 0$ throughout. Hence there is no enhancement of the coupling at the surface. There is ambiguity with regard to where one puts the boundaries and how the thickness of the film is precisely defined. Here we follow the convention that L_0 gives the number of layers with fluctuating spins. In our previous work,[30] we studied the limit of strong adsorption, $|h_1|, |h_2| \to \infty$. In this limit, the spins at the boundary are fixed to either -1 or $+1$. Therefore, we had put the fixed spins on $x_0 = 0$ and $x_0 = L_0 + 1$ to get L_0 layers with fluctuating spins. Note that these fixed spins could also be interpreted as external fields $h_{1,2} = \pm\beta$ acting on the spins at $x_0 = 1$ and $x_0 = L_0$, respectively. In the following, we shall denote the type of boundary conditions by (h_1,h_2). In the literature, the cases $h_1 = 0$ or $h_2 = 0$ are often called free boundary conditions. To be consistent with the literature, we shall denote the strong adsorption limit by $+$ or $-$ in the following. In particular, the two cases studied in Ref. 30 are denoted by $(+,+) \equiv (\beta,\beta)$ and $(+,-) \equiv (\beta, -\beta)$. For the discussion of the behavior of physical quantities near the boundary, it is useful to define the distance from the boundary. To this end, we shall assume that the first boundary is located at $x_0 = 1/2$ and the second one at $x_0 = L_0 + 1/2$. Hence the distance from the first boundary is given by $z = x_0 - 1/2$ and the distance from the second one by $z = -x_0 + L_0 + 1/2$.

To determine the thermodynamic Casimir force, we have measured the energy per area of the film. It is given by

$$E = \frac{1}{L^2}\left\langle \sum_{\langle xy\rangle} s_x s_y \right\rangle. \tag{16}$$

Since the film is invariant under translations in 1 and 2 directions but not in 0 direction, the magnetization depends on x_0. Therefore, we define the magnetization of a slice by

$$m(x_0) = \frac{1}{L^2}\left\langle \sum_{x_1,x_2} s_x \right\rangle. \tag{17}$$

III. PHASE DIAGRAM OF A SEMI-INFINITE SYSTEM

Here we briefly recall the phase diagram of a semi-infinite Ising system as it is discussed, e.g., in the reviews in Refs. 10–12. For the Blume-Capel model, we expect that for $D \lessapprox 2$ the qualitative features of the phase diagram remain unchanged since $D_{\rm tri} = 1.966(2)$ (Ref. 38) for the two-dimensional system and $D_{\rm tri} = 2.0313(4)$ (Ref. 35) for the three-dimensional one.

In Fig. 1, we have sketched the phase diagram for a vanishing external field $h = 0$ and a vanishing surface field $h_1 = 0$. For $\beta > \beta_c$, the spins in the bulk are ordered. As a consequence, the spins at the surface are also ordered. This phase is denoted by C in Fig. 1. At vanishing bulk coupling $\beta = 0$, the spins at the surface decouple completely from those of the bulk. Hence a two-dimensional Ising or Blume-Capel model remains that undergoes a phase transition at $\beta_1 = \beta_{c,2D}$. Starting from the point $(0,\beta_{c,2D})$, there is a line of transitions where the spins at the surface order while those of the bulk remain disordered. This line hits the vertical line at $\beta = \beta_c$ in the so called special or surface-bulk point, which is a tricritical point, that we denote by SB in Fig. 1. In Fig. 1, the phase where both the boundary spins and those of the bulk are disordered is denoted by A while the one with a disordered bulk and an ordered surface is denoted by B. The transitions from phase A to phase C are so called ordinary transitions, while those from phase B to phase C are so called extraordinary transitions. The transitions from phase A to B are so called surface transitions.

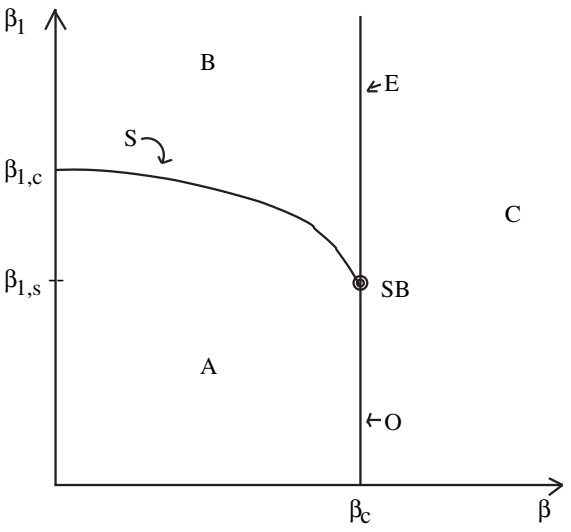

FIG. 1. Sketch of the phase diagram of the semi-infinite system. On the x axis we plot the coupling β of the bulk, and on the y axis we plot the excess coupling β_1 of the surface. A detailed discussion is given in the text.

For $h_1 \neq 0$, the spins at the surface are ordered also for $\beta_1 \leqslant \beta_{1,s}$. In the literature, the transitions from disordered to ordered spins in the bulk for $h_1 \neq 0$ are called normal transitions. In Ref. 39, it has been shown that the normal surface universality class is equivalent to the extraordinary surface universality class.

At the ordinary transition, the external field h_1 at the surface is a relevant perturbation. Hence the RG exponent y_{h_1} associated with the surface field is positive. In the literature, a number of surface critical exponents have been introduced. In the case of the ordinary transition, these can be obtained from y_{h_1} and the bulk RG exponents $y_t = 1/\nu$ and $y_h = (d+2-\eta)/2$ by using scaling relations. In the following, we need

$$\Delta_1 = \nu y_{h_1}, \tag{18}$$

$$\beta_1 = \nu\big(d - 1 - y_{h_1}\big), \tag{19}$$

$$\gamma_1 = \nu\big(2 - d/2 - \eta/2 + y_{h_1}\big). \tag{20}$$

For the definitions and a complete list of these exponents, see the reviews in Refs. 10–12. The numerical values of surface critical exponents for the three-dimensional Ising universality class have been computed by various theoretical methods. Mean-field theory predicts $y_{h_1} = 1/2$. The authors of Ref. 40 quote $y_{h_1} = 0.7363$ as result of their real-space RG method, and the authors of Ref. 41 quote $\gamma_1 = 0.78(2)$ as result of a series expansion, which corresponds to $y_{h_1} = 0.72(3)$. The ϵ expansion gives[42]

$$y_{h_1} = \tfrac{1}{2} + \tfrac{1}{6}\epsilon + \tfrac{31}{321}\epsilon^2 + O(\epsilon^3). \tag{21}$$

Naively inserting $\epsilon = 1$, one gets $y_{h_1} = 0.666\ldots$ and $y_{h_1} = 0.762\ldots$ at $O(\epsilon)$ and $O(\epsilon^2)$, respectively. Using a massive field theory approach, the authors of Ref. 43 obtained $\Delta_1 = 0.45$ from the $[1/1]$ Padé approximant of their two-loop result, which corresponds to $y_{h_1} = 0.714$. Comparing the different Padé approximants that are given in Table 9 of Ref. 43, one might conclude that the uncertainty of the estimate of y_{h_1} is about 0.02. In Table I, we have summarized Monte Carlo results for surface critical exponents. Most of the authors quote an estimate for β_1 and some in addition for γ_1. In those cases in which the authors did not quote a result for y_{h_1}, we have converted the value given for β_1 using the scaling relation (19) and $\nu = 0.630\,02(10)$.

For comparison, we also anticipate our result for y_{h_1} that we obtain in Sec. VI A below. Except for Ref. 48, the estimates for y_{h_1} are larger than ours. In particular, note that the difference between our result and that of Ref. 51 is about six times as large as the combined error.

IV. FINITE-SIZE SCALING APPLIED TO FILMS

In this section, we shall discuss the finite-size scaling behavior of the magnetization profile at the bulk critical point

TABLE I. Monte Carlo results for surface critical exponents for the ordinary phase transition in the three-dimensional Ising universality class. The authors of Ref. 45 quote no final result for γ_1. Here we give the average of the three results given in Table II of Ref. 45. In case the authors do not quote an estimate for y_{h_1}, we have computed it from β_1 and the scaling relation (19). These cases are marked by an asterisk.

Ref.	β_1	γ_1	y_{h_1}
44	0.78(2)		0.762(32)*
45	0.79(2)	0.79(10)	0.746(32)*
46	0.78(2)	0.78(6)	0.762(32)*
47			0.740(15)
48	0.807(4)	0.760(4)	0.719(6)*
49	0.80(1)	0.78(5)	0.730(16)*
50			0.737(5)
51	0.796(1)		0.7374(15)
52	0.795(6)		0.738(10)*
here			0.7249(6)

and thermodynamic Casimir force for arbitrary temperature. The starting point of our considerations is the reduced excess free energy per area of the film,

$$f_{\rm ex}(L_0,t,h_1) = f_{\rm film}(L_0,t,h_1) - L_0 f_{\rm bulk}(t), \tag{22}$$

where $f_{\rm film}(L_0,t,h_1)$ is the reduced free energy of the film per area and $f_{\rm bulk}(t)$ is the reduced bulk free energy density. There is no dependence on h_2, since we consider the limit $h_2 \to \infty$. The singular part of the reduced excess free energy per area has the finite-size scaling behavior,[10–12]

$$f_{{\rm ex},s}(L_0,t,h_1) = L_0^{-d+1} g(t[L_0/\xi_0]^{y_t}, h_1[L_0/l_{\rm ex,nor,0}]^{y_{h_1}}), \tag{23}$$

where we have ignored corrections to scaling at the moment and $d = 3$ is the dimension of the bulk system. We shall define the amplitude $l_{\rm ex,nor,0}$ of the normal extrapolation length $l_{\rm ex,nor}$ below, Eq. (30). Note that the bulk contributions to the nonsingular part of the free energy cancel in Eq. (22). However, there remain contributions from the two surfaces.

A. The magnetization profile at the bulk critical point

In terms of the reduced free energy per area, the magnetization at $x_0 = 1$ is given by

$$\begin{aligned} m_1 &= \frac{\partial f_{\rm ex}(L_0,t,h_1)}{\partial h_1} \\ &= \frac{1}{L^2}\,\frac{1}{Z}\,\frac{\sum_{\{s\}} \exp\left(\cdots + h_1 \sum_{x_1,x_2} s_{(1,x_1,x_2)}\right)}{\partial h_1} \\ &= \frac{1}{L^2}\left\langle \sum_{x_1,x_2} s_{(1,x_1,x_2)} \right\rangle . \end{aligned} \tag{24}$$

In Sec. VI A, we shall determine the value of the RG exponent y_{h_1} from the scaling of m_1 with the thickness L_0 at $h_1 = 0$ and $\beta = \beta_c$. Taking the partial derivative of Eq. (23) with respect to h_1, we get

$$\begin{aligned} m_1 &= \left.\frac{\partial f_{\rm ex}}{\partial h_1}\right|_{t=h_1=0} \\ &= L_0^{-d+1}\left.\frac{\partial g(t[L_0/\xi_0]^{y_t}, h_1[L_0/l_{\rm ex,nor,0}]^{y_{h_1}})}{\partial h_1}\right|_{t=h_1=0} \\ &= L_0^{-d+1} g_{h_1}(0,0)|_{t=h_1=0}[L_0/l_{\rm ex,nor,0}]^{y_{h_1}} = c\, L_0^{-d+1+y_{h_1}}, \end{aligned} \tag{25}$$

where g_{h_1} denotes the partial derivative of g with respect to $x_{h_1} = h_1[L_0/l_{\rm ex,nor,0}]^{y_{h_1}}$. Note that the nonsingular contribution to $f_{\rm ex}$ from the first surface does not feel the breaking of the symmetry by the second surface. Therefore, it is an even function of h_1 and does not contribute to the partial derivative with respect to h_1.

The extrapolation length $l_{\rm ex}$ can be defined by the behavior[10–12]

$$m(x_0) = c\, L_0^{-\beta/\nu}\, \psi(x_0/L_0) \tag{26}$$

of the magnetization profile at the critical point of the bulk system. Note that from scaling relations it follows that $\beta/\nu = (1+\eta)/2$, where $\eta = 0.036\,27(10)$ for the three-dimensional Ising universality class.[36]

In the neighborhood of the surface with spins fixed to $s_x = 1$, one expects that for $z \ll L_0$, where $z = L_0 - x_0 + 1/2$, the magnetization profile does not depend on L_0. Therefore, $\psi(x_0/L_0) = (z/L_0)^{-\beta/\nu}$ and hence[10–12]

$$m(x_0) = c\, z^{-\beta/\nu}. \tag{27}$$

Also at the free boundary we expect that for $z \ll L_0$, where now $z = x_0 - 1/2$, the functional form of the magnetization profile does not depend on L_0. As we have seen above, for a fixed value of z, the magnetization behaves as $m_1 \propto L_0^{-d+1+y_{h_1}}$. Therefore,[10–12]

$$m(x_0) = a\, z^{-\beta/\nu+d-1-y_{h_1}} = a\, z^{(\beta_1-\beta)/\nu}. \tag{28}$$

Since $-\beta/\nu < 0$, the scaling function of the magnetization profile diverges as $z/L_0 \to 0$ at the boundary with fixed spins. On the other hand, since $(\beta_1 - \beta)/\nu > 0$ the scaling function of the magnetization vanishes as $z/L_0 \to 0$ at the free boundary.

Based on this observation, one might define for finite thicknesses L_0 an effective distance from the boundary,

$$z_{\rm eff} = z + l_{\rm ex}, \tag{29}$$

such that the magnetization profile at $z_{\rm eff} = 0$ vanishes for $h_1 = 0$ or diverges in the case of symmetry-breaking boundary conditions. The concept of the extrapolation length has been worked out explicitly for the ordinary transition in the framework of mean-field theory.[10] Also in the Monte Carlo study of the magnetization profile of a semi-infinite system in the extraordinary surface universality class, an extrapolation length had been introduced.[53] The extrapolation length is related with corrections $\propto L_0^{-1}$ discussed in the framework of field theory in Ref. 54. In the following, we shall distinguish between the extrapolation length $l_{\rm ex,ord}$ (where "ord" denotes ordinary surface transition) and $l_{\rm ex,nor}$ (where "nor" denotes normal surface transition) in the case of symmetry-breaking boundary

conditions. The extrapolation length depends on the precise definition of z. Physically, the extrapolation length depends on the details of the microscopic model, in particular on the details of the fields and interactions at the surface. In Sec. VI B, we shall study the behavior of the extrapolation length as a function of the field h_1 at the boundary. One expects[55]

$$l_{\mathrm{ex,nor}}(h_1) = l_{\mathrm{ex,nor},0}\, h_1^{-1/y_{h_1}}, \tag{30}$$

which defines the amplitude $l_{\mathrm{ex,nor},0}$ that we have already used above in Eq. (23).

Capehart and Fisher[56] have argued that the arbitrariness in the definition of the thickness of the film leads to corrections $\propto L_0^{-1}$. These corrections can be eliminated by replacing L_0 in finite-size scaling laws such as Eq. (23) by an effective thickness

$$L_{0,\mathrm{eff}} = L_0 + L_s \tag{31}$$

of the film. Assuming that the corrections due to a surface are caused by a unique irrelevant surface scaling field, the constant L_s should be given by

$$L_s = l_{\mathrm{ex},1} + l_{\mathrm{ex},2}, \tag{32}$$

where $l_{\mathrm{ex},1}$ and $l_{\mathrm{ex},2}$ are the extrapolation lengths at the two surfaces of the film. In Sec. II A 4 of Ref. 27, a similar discussion of the extrapolation length was presented. For a discussion of the effective thickness and further references, see Sec. IV of Ref. 30.

B. Crossover scaling function of the thermodynamic Casimir force

In terms of the reduced excess free energy per area, the thermodynamic Casimir force per area is given by[5]

$$\frac{1}{k_B T} F_{\mathrm{Casimir}} = -\frac{\partial f_{\mathrm{ex}}}{\partial L_0}. \tag{33}$$

Using the finite-size scaling law (23), we arrive at

$$\begin{aligned}\frac{\partial f_{\mathrm{ex},s}(L_0,t,h_1)}{\partial L_0} &= (-d+1)L_0^{-d} g\left(x_t,x_{h_1}\right) + L_0^{-d} y_t t [L_0/\xi_0]^{y_t}\; g_t(x_t,x_h) \\ &\quad + L_0^{-d} y_{h1} h_1 [L_0/l_{\mathrm{ex,nor},0}]^{y_{h1}} g_{h_1}\left(x_t,x_{h_1}\right),\end{aligned} \tag{34}$$

where $x_t = t[L_0/\xi_0]^{y_t}$ and $x_{h_1} = h_1[L_0/l_{\mathrm{ex,nor},0}]^{y_{h1}}$. The partial derivatives of g with respect to x_t and x_{h_1} are denoted by g_t and g_{h_1}, respectively. Note that the analytic part of f_{ex} is due to the surfaces and does not depend on L_0 and therefore does not contribute to the thermodynamic Casimir force. It follows that the thermodynamic Casimir force per area follows the finite-size scaling law[15]

$$F_{\mathrm{Casimir}} = k_B T L_0^{-d} \Theta(t[L_0/\xi_0]^{y_t}, h_1[L_0/l_{\mathrm{ex,nor},0}]^{y_{h1}}), \tag{35}$$

where

$$\begin{aligned}\Theta\left(x_t,x_{h_1}\right) &= (d-1)g\left(x_t,x_{h_1}\right) - y_t t[L_0/\xi_0]^{y_t}\; g_t(x_t,x_h) \\ &\quad - y_{h1} h_1 [L_0/l_{\mathrm{ex,nor},0}]^{y_{h1}} g_{h_1}\left(x_t,x_{h_1}\right).\end{aligned} \tag{36}$$

Taking the nth derivative of the thermodynamic Casimir force with respect to h_1, we get

$$\frac{\partial^n F_{\mathrm{Casimir}}}{\partial h_1^n} = k_B T L_0^{-d} [L_0/l_{\mathrm{ex,nor},0}]^{n y_{h1}} \frac{\partial^n \Theta\left(x_t,x_{h_1}\right)}{\partial x_{h_1}^n}. \tag{37}$$

V. COMPUTING THE THERMODYNAMIC CASIMIR FORCE AND DERIVATIVES WITH RESPECT TO THE EXTERNAL FIELD AT THE SURFACE

On the lattice, we approximate the derivative of the reduced excess free energy per area with respect to the thickness L_0 of the film by a finite difference:

$$\frac{\partial f_{\mathrm{ex}}}{\partial L_0} \approx \Delta f_{\mathrm{ex}}(L_0) = f_{\mathrm{ex}}(L_0+1/2) - f_{\mathrm{ex}}(L_0-1/2), \tag{38}$$

where $L_0+1/2$ and $L_0-1/2$ are positive integers. As suggested by Hucht,[31] we compute this difference of free energies as the integral of the difference of corresponding internal energies:

$$\Delta f_{\mathrm{ex}}(L_0,\beta) = -\int_{\beta_0}^{\beta} \mathrm{d}\tilde{\beta}\, \Delta E_{\mathrm{ex}}(L_0,\tilde{\beta}), \tag{39}$$

where

$$\Delta E_{\mathrm{ex}}(L_0) = E(L_0+1/2) - E(L_0-1/2) - E_{\mathrm{bulk}}. \tag{40}$$

In practice, the integral (39) is computed by using the trapezoidal rule. Our previous experience[30] shows that $\Delta E_{\mathrm{ex}}(L_0)$ has to be computed for about 100 values of β to obtain $\Delta f_{\mathrm{ex}}(L_0,\beta)$ in the whole range of β in which we are interested at the level of accuracy at which we are aiming.

In this work, we compute the Taylor expansion of the thermodynamic Casimir force with respect to the boundary field h_1 around $h_1 = 0$ up to second order. To this end, we compute the first and second derivative of $\Delta f_{\mathrm{ex}}(L_0)$ with respect to h_1. The nth derivatives can be written as

$$\frac{\partial^n \Delta f_{\mathrm{ex}}(L_0,\beta,h_1)}{\partial h_1^n} = -\int_{\beta_0}^{\beta} \mathrm{d}\tilde{\beta}\, \frac{\partial^n \Delta E_{\mathrm{ex}}(L_0,\tilde{\beta},h_1)}{\partial h_1^n}, \tag{41}$$

where

$$\frac{\partial^n \Delta E_{\mathrm{ex}}(L_0,\beta,h_1)}{\partial h_1^n} = \frac{\partial^n E(L_0+1/2,\beta,h_1)}{\partial h_1^n} - \frac{\partial^n E(L_0-1/2,\beta,h_1)}{\partial h_1^n}. \tag{42}$$

Note that there is no bulk contribution, since the internal energy of the bulk does not depend on h_1. In the Monte Carlo simulation, the first derivative can be computed as

$$\frac{\partial E(L_0,\beta,h_1)}{\partial h_1} = \langle \tilde{E} M_1 \rangle - \langle \tilde{E} \rangle \langle M_1 \rangle, \tag{43}$$

where

$$\tilde{E} = \frac{1}{L^2} \sum_{\langle xy \rangle} s_x s_y \tag{44}$$

and

$$M_1 = \sum_{x_1,x_2} s_{(1,x_1,x_2)}. \tag{45}$$

The second derivative is given by

$$\frac{\partial^2 E(L_0,\beta,h_1)}{\partial h_1^2} = \langle \tilde{E} M_1^2 \rangle - 2\langle \tilde{E} M_1 \rangle \langle M_1 \rangle - \langle \tilde{E} \rangle \langle M_1^2 \rangle + 2\langle \tilde{E} \rangle \langle M_1 \rangle^2. \quad (46)$$

Higher derivatives could be computed in a similar way. However, it turns out that the relative statistical error of the second derivative is much larger than that of the first one. Therefore, it seems useless to implement and measure higher derivatives.

VI. MONTE CARLO SIMULATION

First, we simulated films with $(0,+)$ boundary conditions at the bulk critical point for thicknesses up to $L_0 = 64$. Analyzing the data obtained from these simulations, we determined the value of L_s for these boundary conditions and we obtained an accurate result for the RG exponent y_{h_1}. Next, we simulated lattices of the size $L_0 = L = 512$ with $(+,0)$ and $(h_1,0)$ boundary conditions with $h_1 = 0.2$, 0.1, 0.05, and 0.02 at the bulk critical point. From the behavior of the magnetization profile in the neighborhood of the surfaces, we determined the extrapolation length $l_{\mathrm{ex,ord}}$ for free boundary conditions and the extrapolation length $l_{\mathrm{ex,nor}}$ as a function of h_1. Next, we studied $(h_1,-)$ boundary conditions for $h_1 = 0.2$, 0.18, 0.16, 0.15, 0.14, 0.13, 0.12, 0.11, 0.1, 0.09, 0.08, 0.07, 0.06, and 0.05 also at the bulk critical point. From the zero of the magnetization profile, we read off the difference $l_{\mathrm{ex,nor}}(h_1) - l_{\mathrm{ex,nor}}(-)$ of extrapolation lengths. Note that $l_{\mathrm{ex,nor}}(-) = l_{\mathrm{ex,nor}}(+)$ due to symmetry.

Next, we studied the thermodynamic Casimir force per area in the neighborhood of the bulk critical point. To this end, we simulated films of thicknesses $L_0 = 8, 9, 12, 13, 16$, and 17 for about 100 values of β each. Using the data obtained from these simulations, we computed the finite-size scaling function of the thermodynamic Casimir force per area for $(0,+)$ boundary conditions. Furthermore, we computed the Taylor expansion of the thermodynamic Casimir force per area for $(h_1,+)$ boundary conditions to second order around $h_1 = 0$. We simulated $L_0 = 8$ and 9 at $h_1 = 0.03$, 0.06, 0.1, and 0.2 to check for how large values of h_1 and hence of x_{h_1} the Taylor expansion accurately describes the finite-size scaling function $\Theta(x_t, x_{h_1})$. Finally, we studied the approach to the strong adsorption limit as $x_{h_1} \to \infty$.

As in our previous work,[30] we simulated the Blume-Capel model by using a hybrid[57] of local heat-bath updates and cluster updates.[58,59] Since the cluster updates only change the sign of the spins, additional local updates are needed to ensure ergodicity of the compound algorithm. In one cycle of our algorithm, we sweep twice through the lattice using the local heat bath algorithm followed by one or more cluster updates. In one sweep, we run through the lattice in typewriter fashion, performing heat bath updates site by site. We have always performed a cluster update, in which all spins are flipped that are not frozen to the boundary. For a detailed discussion, see Sec. V A of Ref. 30. Note that here, in contrast to Ref. 30, we have applied this type of cluster update also to systems with $(+,-)$ boundary conditions. To this end, we had to adapt the implementation of the cluster search; we had to allow for the possibility that two spins in the cluster frozen to the boundary might have different signs. Furthermore, we generalized the cluster update to the case of a finite external field h_1 at the surface. A spin at the boundary freezes to the external field with the probability $p_f = 1 - p_d$, where

$$p_d = \min[1, \exp(-2h_1 s_x)]. \quad (47)$$

In the case of large systems, discussed in Secs. VI B 1 and VI B 2 below, we performed in addition single-cluster updates.[59] In all our simulations, we have used the SIMD-oriented Fast Mersenne Twister algorithm[60] as a pseudo-random-number generator.

A. Simulations at the bulk critical point

First, we simulated films with $(0,+)$ boundary conditions at our estimate of the bulk critical point $\beta_c = 0.387\,721\,735$.[36] Since the fixed spins at the second surface act effectively as an external field for the effectively two-dimensional system, the correlation length of the film stays finite at any value of β. This means that for a given thickness L_0, finite L effects decay $\propto \exp(-L/\xi_{\mathrm{film}})$ for sufficiently large values of L. Hence we can choose L such that finite-size effects are much smaller than the statistical errors and therefore can be ignored in the analysis of our Monte Carlo data. To check which values of L are needed to this end, we have performed simulations for the thickness $L_0 = 6$ using $L = 6$, 7, 8, 9, 10, 11, 12, 13, 14, 15, 16, 18, 20, 24, 32, and 48. For each of these lattice sizes, we have performed 10^9 or more update cycles. As a check, we have simulated films with thickness $L_0 = 12$ and $L = 24$, 24, 28, 32, 40, 48, 56, 64, and 96, where we performed 10^8 update cycles throughout. We have studied the behavior of the second moment correlation length, the magnetization at the surface m_1, and the energy per area of the film E and its first and second derivative with respect to h_1.

Here we use the same definition of the second moment correlation length as in Ref. 30. See, in particular, Sec. III C of Ref. 30. The disadvantage of this definition of the second moment correlation length is that as soon as more than one eigenstate of the transfer matrix contributes to the correlation function, corrections to the $L \to \infty$ limit only decay $\propto L^{-2}$. In Fig. 2, we have plotted the second moment correlation length obtained with the pairs of wave vectors $[(0,0),(0,1)]$ and $[(1,0),(1,1)]$ as a function of L^{-2}. While the estimate obtained by using the pair of wave vectors $[(1,0),(1,1)]$ is monotonically increasing with increasing L, the estimate obtained by using the pair $[(0,0),(0,1)]$ displays a minimum close to $L = 12$. The value at this minimum is about 0.993 times the asymptotic value.

Fitting the results obtained for $L = 24$, 32, and 48 with the *Ansatz* $\xi_{\mathrm{2nd}}(L) = \xi_{\mathrm{2nd}} + aL^{-2}$, we get $\xi_{\mathrm{2nd}} = 1.6988(6)$ and 1.6990(5) for the choices $[(0,0),(1,0)]$ and $[(1,0),(1,1)]$, respectively.

Next, we analyzed the energy per area, its first and second derivative with respect to h_1, and the magnetization m_1 at the surface. These quantities should converge with exponentially small corrections as $L \to \infty$. We have fitted these quantities with the *Ansatz* $A(L) = A(\infty) + c_A \exp(-L/\xi_{\mathrm{film}})$, where we have taken our result for the second moment correlation length $\xi_{\mathrm{2nd}} = 1.70$, which should not be much smaller than

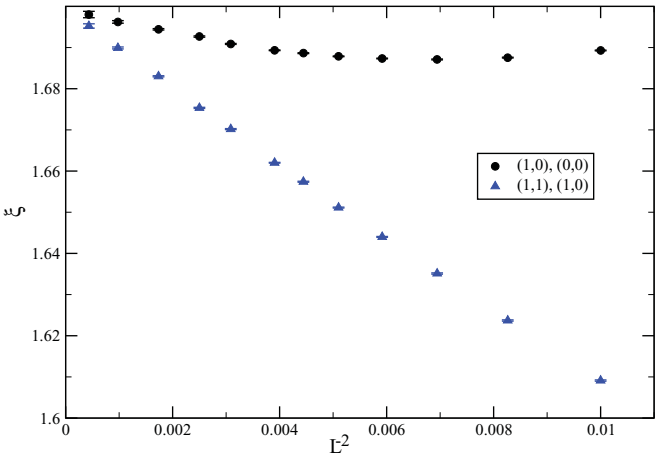

FIG. 2. (Color online) We plot ξ_{2nd} as a function of L^{-2}, where L is the linear extension in the transversal directions, for films of the thickness $L_0 = 6$. We have computed the second-moment correlation length by using the pairs of wave vectors [(0,0),(1,0)] (circles) and [(1,0),(1,1)] (triangles).

the exponential correlation length that is actually needed here. Fitting all data with $L \geqslant 16$, we find for the magnetization at the boundary $\chi^2/\mathrm{DOF} = 4.55/4$, $m_1(\infty) = 0.125\,017\,5(6)$, and $c_{m_1} = -0.237(25)$. This means that for $L \approx 11\xi_{\mathrm{film}}$, the deviation from the limit $L \to \infty$ has about the same size as the statistical error that we have reached here for $L_0 = 6$. Note that below, for larger thicknesses, the number of measurements is more than a factor of 10 smaller than for $L_0 = 6$. Analyzing the energy per area and its first and second derivative with respect to h_1, we find that for $L \approx 10\xi_{\mathrm{film}}$ the deviation from the limit $L \to \infty$ has about the same size as the statistical error. Analyzing our results for the thickness $L_0 = 12$, we find consistently that for m_1 and the energy per area and its first and second derivative with respect to h_1, the deviation from the limit $L \to \infty$ has about the same size as the statistical error for $L \approx 10\xi_{\mathrm{film}}$. As we shall see below, $\xi_{\mathrm{film}} \approx 0.225(L_0 + 1.43)$. Therefore, for $L = 4L_0$, which we have used below, the deviation from the limit $L \to \infty$ should be clearly smaller than the statistical error and can hence be ignored.

Next, we simulated films for a large number of thicknesses up to $L_0 = 64$ at $\beta = 0.387\,721\,735$, using $L = 4L_0$ throughout. For the thicknesses $L_0 = 6$, 7, 8, 9, 10, 11, 12, 13, 14, 15, 16, 18, 20, 22, and 24, we performed 10^8 update cycles throughout, and 7.6×10^7, 10^8, 8.7×10^7, 6.5×10^7, 4.3×10^7, 2.6×10^7, and 2.5×10^7 update cycles for $L_0 = 28$, 32, 36, 40, 48, 56, and 64, respectively. These simulations took about 18 months of CPU time on a single core of a Quad-Core AMD Opteron(tm) Processor 2378 running at 2.4 GHz.

We fitted the data of the magnetization m_1 at the surface with free boundary conditions with the *Ansatz*

$$m_1 = b\,(L_0 + L_s)^{2-y_{h_1}}, \tag{48}$$

where b and y_{h_1} are the parameters of the fit and

$$m_1 = b\,(L_0 + L_s)^{2-y_{h_1}} \times [1 + c\,(L_0 + L_s)^{-2}], \tag{49}$$

where now c is an additional parameter, to obtain some control on subleading corrections. We have taken into account all data obtained for the thicknesses $L_0 \geqslant L_{0,\mathrm{min}}$. Fitting our data with the *Ansatz* (48), we get acceptable fits already for $L_{0,\mathrm{min}} = 10$: $b = 1.6131(13)$, $L_s = 1.4289(33)$, $y_{h_1} = 0.724\,93(20)$, and $\chi^2/\mathrm{DOF} = 13.2/15$. Fitting with *Ansatz* (49), we get for $L_{0,\mathrm{min}} = 6$ the results $b = 1.6109(22)$, $L_s = 1.4166(86)$, $y_{h_1} = 0.725\,20(31)$, $c = -0.09(4)$, and $\chi^2/\mathrm{DOF} = 18.1/18$.

We arrive at the final estimates

$$b = 1.613(4), \tag{50}$$

$$L_s = 1.43(2), \tag{51}$$

$$y_{h_1} = 0.7249(6), \tag{52}$$

where the central result is taken from the fit with the *Ansatz* (48) and $L_{0,\mathrm{min}} = 10$. The error bar is chosen such that also the result for the fit with subleading corrections (49) is covered. We have also estimated the error induced by the uncertainty of our estimate of the inverse bulk critical temperature β_c. To this end, we first determined the derivative of m_1 with respect to β for $L_0 = 8$,9,12,13,16, and 17, where we performed simulations for many values of β. We extrapolated these results to other values of L_0 assuming $\partial m_1/\partial\beta \propto (L_0 + L_s)^{2-y_{h_1}+y_t}$. Using this, we computed m_1 at $\beta = \beta_c + \mathrm{error} = 0.387\,721\,76$ and we redid the fits performed above. We found that the deviations of the results for $\beta = 0.387\,721\,76$ from those for $\beta = 0.387\,721\,735$ are much smaller than the errors quoted in Eqs. (50)–(52).

Next, we analyzed the second moment correlation length obtained by using the pair [(1,0),(1,1)] of wave vectors. Following the discussion above, finite L effects might still be at the level of 1% for our choice $L = 4L_0$. Since this effect is essentially the same for all thicknesses, it mainly effects the parameter c in the two equations below. First, we fitted our data with the *Ansatz*

$$\xi_{2nd} = c\,(L_0 + L_s), \tag{53}$$

where c and L_s are the parameters of the fit. Using $L_{0,\mathrm{min}} = 8$, we obtain $c = 0.224\,35(9)$, $L_s = 1.487(6)$, and $\chi^2/\mathrm{DOF} = 19.2/18$. Fitting instead with the *Ansatz*

$$\xi_{2nd} = c\,(L_0 + L_s) \times [1 + b\,(L_0 + L_s)^{-2}], \tag{54}$$

we get for $L_{0,\mathrm{min}} = 6$ the results $c = 0.224\,76(16)$, $L_s = 1.422(20)$, $b = 0.48(12)$, and $\chi^2/\mathrm{DOF} = 15.0/19$. We conclude that the estimate for L_s obtained from the finite-size scaling behavior of ξ_{2nd} is consistent with but less precise than that obtained from the finite-size scaling behavior of m_1.

Finally, we fitted the energy per area with the *Ansatz*

$$E = L_0 E_{ns} + E_{ns,s} + c\,(L_0 + L_s)^{-2+1/\nu}, \tag{55}$$

where we used $E_{ns} = 0.602\,111(1)$ (Ref. 37) and $\nu = 0.630\,02(10)$ as input. Starting from our smallest thicknesses, we get acceptable fits: For $L_{0,\mathrm{min}} = 6$ we obtain $c = -3.5916(7)$, $L_s = 1.4136(21)$, $E_{ns,s} = 3.0644(2)$, and $\chi^2/\mathrm{DOF} = 18.8/19$. As a check, we also fitted with the *Ansatz*

$$E = L_0 E_{ns} + E_{ns,s} + c\,(L_0 + L_s)^{-2+1/\nu} \times [1 + b\,(L_0 + L_s)^{-2}], \tag{56}$$

where we included subleading corrections. For $L_{0,\mathrm{min}} = 6$, we get $c = -3.5930(15)$, $L_s = 1.423(12)$, $E_{ns,s} = 3.0646(2)$, $b = 0.017(23)$, and $\chi^2/\mathrm{DOF} = 18.4/18$.

We also redid the fits for shifted values of E_{ns} and ν. Since we have seen above in the case of m_1 that the uncertainty of β_c is negligible, we have skipped this check here. Taking all these results into account, we arrive at the final estimates,

$$E_{ns,s} = 3.064(1), \tag{57}$$

$$L_s = 1.42(2), \tag{58}$$

$$c = 3.592(3). \tag{59}$$

In particular, we notice that the estimate of L_s is fully consistent with that obtained above from the analysis of the magnetization m_1 at the boundary. In the following, we shall use $L_s = 1.43(2)$ as obtained from the analysis of the magnetization m_1 at the free boundary.

B. The extrapolation length

First we have simulated lattices with $(h_1,0)$ boundary conditions of the size $L_0 = L = 512$ at $\beta = 0.387\,721\,735$ using $h_1 = \beta_c$, 0.2, 0.1, 0.05, and 0.02. For this geometry, one expects strong finite L effects. However, these should not alter the behavior in the neighborhood of the boundary that we study here. In all cases, we performed 2.6×10^5 update cycles. In total, these simulations took about 7 months of CPU time on a single core of a Quad-Core AMD Opteron(tm) Processor 2378 running at 2.4 GHz.

1. Behavior of the magnetization at the free boundary

Following the discussion of Sec. VI A, we determined the extrapolation length $l_{\mathrm{ex,ord}}$ by fitting our data for the magnetization profile with the *Ansatz*

$$m(z) = c\,(z + l_{\mathrm{ex,ord}})^{(\beta_1-\beta)/\nu}, \tag{60}$$

where z gives the distance from the boundary as defined in Sec. II A, a few lines above Eq. (16). To this end, we computed the ratios

$$r(z) = m(z + 1/2)/m(z - 1/2) \tag{61}$$

to eliminate the constant in Eq. (60). It turns out that cross-correlations of these ratios are relatively small. Therefore, for simplicity, we fitted our data for these ratios taking only their statistical error into account, ignoring cross-correlations. The statistical errors of the fit parameters were computed by using a jackknife procedure on top of the whole analysis, providing us with correct statistical errors for the results.

First, we fitted our data with the *Ansatz*

$$r(z) = \left(\frac{z + l_{\mathrm{ex,ord}} + 1/2}{z + l_{\mathrm{ex,ord}} - 1/2}\right)^{(\beta_1-\beta)/\nu}, \tag{62}$$

where the free parameters of the fit are the extrapolation length $l_{\mathrm{ex,ord}}$ and the exponent $(\beta_1 - \beta)/\nu$. We performed a large number of fits with various choices of the range $z_{\min} \leqslant z \leqslant z_{\max}$ of distances from the boundary that are taken into account, for all values of h_1 that we have simulated. The results for different h_1 are consistent among each other. In Fig. 3, we show our results for the exponent $(\beta_1 - \beta)/\nu$ for the choice $z_{\max} = 3z_{\min}$ as a function of $z_{\min}$, where we averaged over all values of h_1 that we have simulated. The error that we give is purely statistical. For comparison, we plot the estimate of $(\beta_1 - \beta)/\nu = 2 - y_{h_1} - (1 + \eta)/2 = 0.7570(7)$ obtained by using our estimate of y_{h_1}, Eq. (52), and $\eta = 0.036\,27(10)$.[36]

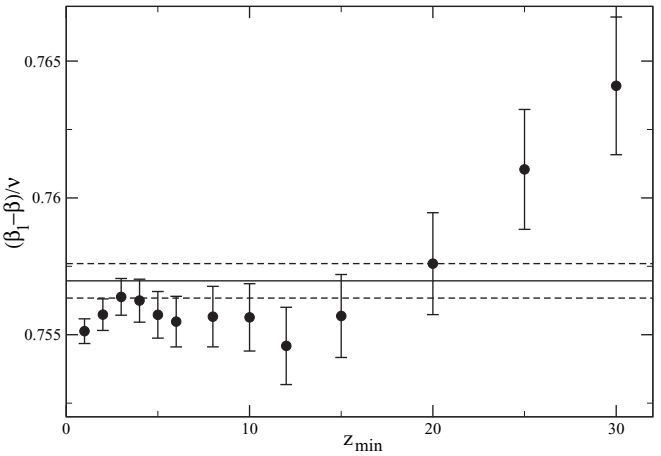

FIG. 3. We plot the estimate of $(\beta_1 - \beta)/\nu$ obtained by fitting with *Ansatz* (62) as a function of $z_{\min}$ (filled circles). In these fits, distances $z_{\min} \leqslant z \leqslant 3z_{\min}$ from the boundary are taken into account. We have averaged the results over all values of h_1 that we have simulated. These results are compared with $(\beta_1 - \beta)/\nu = 2 - y_1 - (1 + \eta)/2 = 0.7570(7)$ obtained by using $y_{h_1} = 0.7249(6)$, see the previous section, and $\eta = 0.036\,27(10)$,[36] where the central value is depicted by the solid line and the error bars are indicated by the dashed lines.

We find that for $z_{\min} = 5$ up to 30, the estimates obtained from the behavior of the magnetization profile in the neighborhood of the surface are consistent with but less precise than the one obtained using the estimate of y_{h_1} in the previous section. Therefore, to determine our final result for the extrapolation length $l_{\mathrm{ex,ord}}$, we have fixed $(\beta_1 - \beta)/\nu = 0.7570(7)$. Fitting the data for $r(z)$ averaged over all values of h_1 that we have simulated in the range $5 \leqslant z \leqslant 30$, we arrive at

$$l_{\mathrm{ex,ord}} = 0.48(1), \tag{63}$$

where the error is dominated by the uncertainty of $(\beta_1 - \beta)/\nu$.

2. Normal extrapolation length as a function of h_1: Part 1

Following the discussion of Sec. IV A, the magnetization in the neighborhood of the surface behaves as

$$m(z,h_1) \propto [z + l_{\mathrm{ex,nor}}(h_1)]^{-\beta/\nu}, \tag{64}$$

where z gives the distance from the boundary. Also in the case of symmetry-breaking boundary conditions, we have computed ratios (61) of the magnetization of neighboring slices. These behave as

$$r(z) = \left(\frac{z + l_{\mathrm{ex,nor}} + 1/2}{z + l_{\mathrm{ex,nor}} - 1/2}\right)^{-\beta/\nu}. \tag{65}$$

Here we have solved Eq. (65) with respect to $l_{\mathrm{ex,nor}}$ for a single value of z, where we have used $\beta/\nu = 0.518\,135$. For $h_1 = \beta_c$, we find for $z \approx 15$ only a small dependence of the result on z. We read off $l_{\mathrm{ex,nor}} = 0.96(2)$. In a similar way, we have determined the extrapolation length for the other values of h_1. Our results are summarized in Table II.

In Ref. 36, we determined $L_s = 1.9(1)$ for $(+,+)$ and $(+,-)$ boundary conditions analyzing films of thicknesses up to

TABLE II. The extrapolation length $l_{\mathrm{ex,nor}}$ is obtained for various values of h_1 by analyzing the behavior of the magnetization profile near the surface. For a discussion, see the text.

h_1	$l_{\mathrm{ex,nor}}$
β_c	0.96(2)
0.2	2.25(3)
0.1	5.56(4)
0.05	14.0(2)
0.02	≈ 45

$L_0 = 32$ at the critical point of the bulk system. Now we have added for $(+,+)$ boundary condition simulations for the thicknesses $L_0 = 48$, 64, and 96. This allows us to improve the accuracy of our estimate. Now we find $L_s = 1.90(5)$. This result is in perfect agreement with $L_s = 2l_{\mathrm{ex,nor}}(\beta_c) = 1.92(4)$ obtained here.

For $(0,+)$ boundary conditions, we find $L_s = l_{\mathrm{ex,ord}} + l_{\mathrm{ex,nor}}(\beta_c) = 0.48(1) + 0.96(2) = 1.44(3)$, which is in perfect agreement with the result given in Eq. (51) above.

3. *Normal extrapolation length as a function of h_1: Part 2*

Here we have simulated systems with $h_1 h_2 < 0$, where $h_2 = -\beta_c$, corresponding to fixed spins $s_x = -1$ at $x_0 = L_0 + 1$, and various values of h_1. For such a choice of boundary conditions, the magnetization profile takes positive values in the neighborhood of the first surface and negative ones in the neighborhood of the second surface. Therefore, in between, the magnetization profile vanishes at $x_{0,\mathrm{zero}}$, which depends on h_1 and h_2. The distance of this zero from the first boundary is given by $x_{0,\mathrm{zero}} - 1/2$ and from the second boundary by $L_0 - x_{0,\mathrm{zero}} + 1/2$. Our basic assumption is that the zero of the magnetization indicates the physical middle of the system. Hence the distances of the zero from the effective positions of the first and the second boundary should be the same:

$$x_{0,\mathrm{zero}} - 1/2 + l_{\mathrm{ex,nor}}(h_1) = L_0 - x_{0,\mathrm{zero}} + 1/2 + l_{\mathrm{ex,nor}}(h_2) \tag{66}$$

and hence

$$\Delta l_{\mathrm{ex,nor}}(h_1,h_2) = l_{\mathrm{ex,nor}}(h_1) - l_{\mathrm{ex,nor}}(h_2) = L_0 + 1 - 2x_{0,\mathrm{zero}}. \tag{67}$$

To define the zero of the magnetization, we have linearly interpolated the magnetization profile. Throughout we simulate lattices with $L = 4L_0$. First we have simulated at $h_1 = 0.2$, 0.1, and 0.05, using a large number of thicknesses L_0. Our results are summarized in Table III. Apparently, $\Delta l_{\mathrm{ex,nor}}$ converges with an increasing thickness L_0. Numerically, corrections to the $L_0 \to \infty$ limit are compatible with an exponential decay. However, we cannot strictly exclude powerlike corrections. For $h_1 = 0.2$, our results for $L_0 \geqslant 20$ are compatible within the statistical error. In the case of $h_1 = 0.1$, the results for $L_0 = 40$ and 48 are compatible. The result for $L_0 = 64$ is larger by about twice the combined statistical error than that for $L_0 = 48$. For $h_1 = 0.05$, the results for $L_0 = 120$ and 160 are compatible. It is natural to assume that the thickness L_0 needed to obtain $\Delta l_{\mathrm{ex,nor}}$ with a given relative error is proportional to the extrapolation length $l_{\mathrm{ex,nor}}(h_1)$. Using $l_{\mathrm{ex,nor}}(\beta_c) = 0.96(2)$ obtained in the preceding section, we conclude that for $L_0 \gtrapprox 10 l_{\mathrm{ex,nor}}$ the deviation of $\Delta l_{\mathrm{ex,nor}}$ from its $L_0 \to \infty$ limit is less than the statistical error that we have reached here. Next, we simulated at $h_1 = 0.18$, 0.16, 0.15, 0.14, 0.13, 0.12, 0.11, 0.09, 0.08, 0.07, and 0.06 for a single thickness L_0 each. The thicknesses L_0 and the estimates for $\Delta l_{\mathrm{ex,nor}}$ are given in Table III. Throughout, $L_0 > 10 l_{\mathrm{ex,nor}}$ holds. For each of the simulations given in Table III, we performed about 10^6 update cycles. In total, these simulations took about 8 months of CPU time on a single core of a Quad-Core AMD Opteron(tm) Processor 2378 running at 2.4 GHz. Note that the results obtained here are consistent with those of the previous section. Taking the numbers from Table II, we get $\Delta l_{\mathrm{ex,nor}} = 1.29(5)$, 4.60(6), and 13.04(22) for $h_1 = 0.2$, 0.1, and 0.05, which is perfectly consistent with the results of the present section, given in Table III.

TABLE III. The difference of the extrapolation lengths $\Delta l_{\mathrm{ex,nor}}(h_1,h_2) = l_{\mathrm{ex,nor}}(h_1) - l_{\mathrm{ex,nor}}(h_2)$, where $h_2 = -\beta_c$ as a function of h_1. For a discussion, see the text

h_1	L_0	$\Delta l_{\mathrm{ex,nor}}$
0.2	10	1.2642(21)
0.2	12	1.2748(25)
0.2	14	1.2829(27)
0.2	16	1.2889(32)
0.2	18	1.2852(35)
0.2	20	1.2955(38)
0.2	22	1.2989(42)
0.2	24	1.2938(44)
0.2	28	1.2932(54)
0.2	32	1.2941(62)
0.18	28	1.6182(47)
0.16	32	2.0434(61)
0.15	36	2.313(7)
0.14	42	2.606(9)
0.13	48	2.969(9)
0.12	54	3.401(10)
0.11	60	3.925(11)
0.1	16	4.187(4)
0.1	20	4.330(5)
0.1	24	4.407(6)
0.1	28	4.461(6)
0.1	32	4.488(7)
0.1	40	4.546(8)
0.1	48	4.543(10)
0.1	64	4.579(14)
0.09	80	5.399(13)
0.08	92	6.485(22)
0.07	110	7.917(25)
0.06	140	9.892(35)
0.05	24	10.194(7)
0.05	32	11.108(9)
0.05	40	11.682(11)
0.05	48	12.060(13)
0.05	56	12.279(16)
0.05	64	12.492(17)
0.05	80	12.668(21)
0.05	120	12.892(29)
0.05	160	12.899(42)

From Eq. (30) it follows that

$$\Delta l_{\mathrm{ex,nor}} = l_0 + l_{\mathrm{ex,nor},0}|h_1|^{-1/y_{h_1}}, \tag{68}$$

where naively $l_0 = l_{\mathrm{ex,nor}}(\beta_c)$. However, since $l_{\mathrm{ex,nor}}$ depends on the precise definition of the thickness of the lattice, we keep the offset l_0 as a free parameter here.

It turns out that for the range of h_1 that we have simulated here, analytic corrections have to be taken into account. Therefore, we have fitted our results for the difference of the extrapolation length with the *Ansatz*

$$\Delta l_{\mathrm{ex,nor}} = l_0 + l_{\mathrm{ex,nor},0}\left|h_1 + a h_1^3\right|^{-1/y_{h_1}}, \tag{69}$$

where the amplitude $l_{\mathrm{ex,nor},0}$, the offset l_0, and the correction amplitude a are the parameters of the fit. Note that there should be no term $\propto h_1^2$ since $l_{\mathrm{ex,nor}}(h_1) = l_{\mathrm{ex,nor}}(-h_1)$. We set $y_{h_1} = 0.7249(6)$ as obtained in Sec. VI A. In addition, we have fitted with

$$\Delta l_{\mathrm{ex,nor}} = l_0 + l_{\mathrm{ex,nor},0}\left|h_1 + a h_1^3 + b h_1^5\right|^{-1/y_{h_1}} \tag{70}$$

to check for systematic errors due to the truncation of the Wegner expansion. Alternatively, we have also fitted with

$$\Delta l_{\mathrm{ex,nor}} = l_0 + l_{\mathrm{ex,nor},0}|h_1|^{-1/y_{h_1}} \times \left(1 + \tilde{a} h_1^2\right) \tag{71}$$

and

$$\Delta l_{\mathrm{ex,nor}} = l_0 + l_{\mathrm{ex,nor},0}|h_1|^{-1/y_{h_1}} \times \left(1 + \tilde{a} h_1^2 + \tilde{b} h_1^4\right). \tag{72}$$

Fitting with the *Ansätze* (69) and (71), we get acceptable values of χ^2/DOF starting from $h_{1,\max} = 0.2$, i.e., taking all data into account. Discarding data with large h_1, the result for $l_{\mathrm{ex,nor},0}$ is slightly decreasing and also χ^2/DOF is further decreasing. For example, fitting with *Ansatz* (69) and taking $h_{1,\max} = 0.14$, we get $l_{\mathrm{ex,nor},0} = 0.2133(9)$, $l_0 = 0.04(14)$, $a = 6.9(2.2)$, and $\chi^2/\mathrm{DOF} = 1.72/7$. Taking into account the variation of the results over various *Ansätze* that we have used and the uncertainty of y_{h_1}, we arrive at

$$l_{\mathrm{ex,nor},0} = 0.213(3), \tag{73}$$

which we shall use in the following.

C. The thermodynamic Casimir force

We computed the thermodynamic Casimir force per area and its first and second partial derivative with respect to h_1 for $(0,+)$ boundary conditions for the thicknesses $L_0 = 8.5$, 12.5, and 16.5. To this end, we simulated films of the thicknesses $L_0 = 8$, 9, 12, 13, 16, and 17. For most of the simulations, we used $L = 32$ for $L_0 = 8$ and 9, $L = 48$ for $L_0 = 12$ and 13, and $L = 64$ for $L_0 = 16$ and 17. The correlation length of the film displays a single maximum at a temperature slightly below the critical temperature of the bulk system. The correlation length at the maximum is larger by at most one per mille than at the critical point of the bulk system. Therefore, our choice of L should ensure that finite L effects of the energy per area and its first and second partial derivative with respect to h_1 can be safely ignored. At β values that are much smaller or larger than β_c, we have used smaller values of L. Throughout, we have checked that $L > 10\xi_{\mathrm{film}}$ is fulfilled with a clear safety margin. For $L_0 = 8$ and 9, we simulated at 85 values of the inverse temperature in the range $0.25 \leqslant \beta \leqslant 0.5$, for $L_0 = 12$ and 13 at 124 values in the range $0.3 \leqslant \beta \leqslant 0.42$, and for $L_0 = 16$ and 17 at 112 values in the range $0.34 \leqslant \beta \leqslant 0.406$. The difference between neighboring β values is adapted to the problem: It is the smallest close to β_c. We performed 10^8 update cycles for $L_0 = 8$, 9, 12, and 13 and 2×10^8 update cycles for $L_0 = 16$ and 17 for each value of β. In total, these simulations took about 10 years of CPU time on a single core of a Quad-Core AMD Opteron(tm) Processor 2378 running at 2.4 GHz.

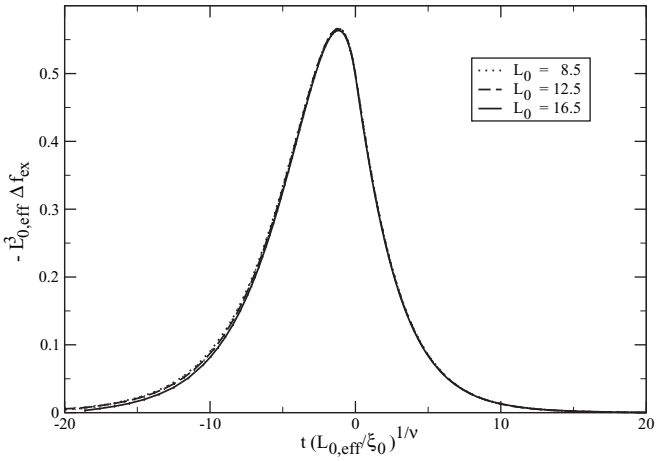

FIG. 4. We plot $-L_{0,\mathrm{eff}}^3 \Delta f_{\mathrm{ex}}$ as a function of $t(L_{0,\mathrm{eff}}/\xi_0)^{1/\nu}$ for $(0,+)$ boundary conditions for the thicknesses $L_0 = 8.5$, 12.5, and 16.5. To this end, we have used $L_{0,\mathrm{eff}} = L_0 + L_s$ with $L_s = 1.43$, $\xi_0 = 0.2282$, and $\nu = 0.63002$.

Using the estimates of the energy per area obtained from these simulations, we computed the thermodynamic Casimir force per area as discussed in Sec. V. In Fig. 4, we have plotted $-L_{0,\mathrm{eff}}^3 \Delta f_{\mathrm{ex}}$ as a function of $t(L_{0,\mathrm{eff}}/\xi_0)^{1/\nu}$, where we have used $L_{0,\mathrm{eff}} = L_0 + L_s$, with $L_s = 1.43$ obtained above in Sec. VI A. We do not show statistical errors in Fig. 4, since they are comparable with the thickness of the lines. The curves for $L_0 = 8.5$, 12.5, and 16.5 fall quite nicely on top of each other. Only for $x \lessapprox -7$, in the low-temperature phase, do we see a small discrepancy between the result for $L_0 = 8.5$, 12.5, and 16.5, which might be attributed to analytic corrections. We conclude that we have obtained a good approximation of the finite-size scaling function $\theta_{(0,+)}$.

Throughout $\theta_{(0,+)}$ is positive, which means that the thermodynamic Casimir force is repulsive. The scaling function $\theta_{(0,+)}$ has a single maximum. We have determined the position of this maximum from the zero of ΔE. We found $\beta_{\max} = 0.390\,69(2)$, $0.389\,443(10)$, and $0.388\,874(6)$ for $L_0 = 8.5$, 12.5, and 16.5, respectively. It follows that $x_{t,\max} = t_{\max}(L_{0,\mathrm{eff}}/\xi_0)^{1/\nu} = -1.184(13)$, $-1.175(11)$, and $-1.174(10)$ for $L_0 = 8.5$, 12.5, and 16.5, respectively. The error bar includes the uncertainties of $\beta_{\max}$, L_s, and ν. Note that the results obtained from the three different thicknesses are consistent. Next, we determined the value of the scaling function at the maximum. We obtained $-L_{0,\mathrm{eff}}^3 \Delta f_{\mathrm{ex}}(x_{t,\max}) = 0.567(4)$, $0.566(3)$, and $0.564(3)$ for $L_0 = 8.5$, 12.5, and 16.5, respectively. The error is dominated by the uncertainty of L_s. The results obtained from the three different thicknesses are consistent. As a final result, we take

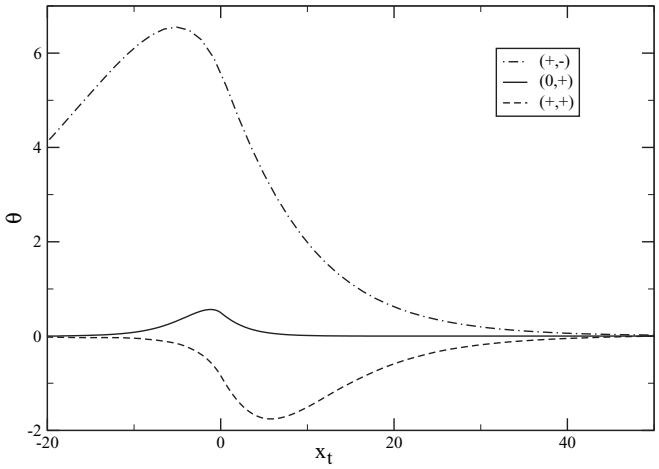

FIG. 5. We plot our result for the finite-size scaling function $\theta_{(0,+)}$ along with those for $\theta_{(+,+)}$ and $\theta_{(+,-)}$ obtained in Ref. 30.

the one obtained from $L_0 = 16.5$:

$$x_{t,\max} = -1.174(10), \quad \theta_{(0,+),\max} = 0.564(3). \tag{74}$$

At the critical point of the bulk system, the finite-size scaling function assumes the value

$$\theta_{(0,+)}(0) = 0.497(3), \tag{75}$$

where the error is dominated by the uncertainty of L_s. This result can be compared with $\theta_{(0,+)}(0) = 0.33$, 0.416, and 0.375(14) obtained by using the ϵ expansion, and Monte Carlo simulations of the Ising model.[61] Similar to the case of $(+,+)$ and $(+,-)$ boundary conditions,[30] we see a large deviation of the results of Krech from ours.

In Fig. 5, we compare the finite-size scaling function of the thermodynamic Casimir force per area for $(0,+)$ boundary conditions with those of $(+,+)$ and $(+,-)$ boundary conditions that we obtained in Ref. 30.

In the high-temperature phase and around the bulk critical point, the absolute value of $\theta_{(0,+)}$ is smaller than that of $\theta_{(+,+)}$, while in the low-temperature phase for $x_t \lessapprox -1.1$ it becomes larger. The value of $\theta_{(0,+)}$ is much smaller than that of $\theta_{(+,-)}$ throughout.

As discussed in Ref. 61 [see, in particular, Eq. (3.6) and Appendix A of Ref. 61], in the mean-field approximation there is a simple relation between the scaling functions $\theta_{(+,-)}$ and $\theta_{(+,0)}$. For $(+,-)$ boundary conditions, the magnetization vanishes in the middle of the film. Hence, ignoring fluctuations, a film of thickness $2L_0$ with $(+,-)$ boundary conditions is composed of two films of thickness L_0, where one has $(+,0)$ and the other $(0,-)$ boundary conditions. Furthermore, $(0,+)$, $(+,0)$, and $(0,-)$ boundary conditions are equivalent. Therefore,

$$\theta_{\mathrm{MF},(0,+)}(x_t) = 2^{-d}\theta_{\mathrm{MF},(+,-)}(2^{1/\nu}x_t). \tag{76}$$

For less than four dimensions, one expects deviations from this relation. Indeed, for the Ising bulk universality class, the ratio of Casimir amplitudes

$$\frac{\Delta_{(+,-)}}{\Delta_{(0,+)}} = 16(1 - 0.481\epsilon + \cdots) \tag{77}$$

obtained by using the ϵ expansion[61] clearly differs from $2^{4-\epsilon} = 16(1 - 0.6931\ldots\epsilon + \cdots)$ obtained from Eq. (76). Note that the Casimir amplitude is given by $2\Delta_{(b_1,b_2)} = \theta_{(b_1,b_2)}(0)$. For two dimensions, one obtains from conformal field theory[62]

$$\frac{\Delta_{(+,-)}}{\Delta_{(+,0)}} = \frac{23}{2}, \tag{78}$$

which is almost three times as large as the factor 4 predicted by Eq. (76).

Taking our numerical data, we find for $x_t > 0$, i.e., in the high-temperature phase, $\theta_{(+,0)}(x_t) \approx 0.7 \times 2^{-3}\theta_{(+,-)}(2^{1/0.630\,02}x_t)$, while in the low-temperature phase, one gets $\theta_{(+,0)}(x_t) \approx 2^{-3}\theta_{(+,-)}(2^{1/0.630\,02}x_t) - 0.3$ in the range $-10 < x_t < -3$. This means that Eq. (76) does not provide a quantitatively accurate relation between the scaling functions $\theta_{(+,0)}(x_t)$ and $\theta_{(+,-)}(x_t)$ in the three-dimensional case.

The most striking observation is that in the high-temperature phase, $\theta_{(0,+)}$ decays, with increasing x_t, much faster to zero than $\theta_{(+,+)}$ and $\theta_{(+,-)}$ do. This behavior can be explained by using the transfer-matrix formalism. For a discussion of the transfer-matrix formalism applied to the problem of the thermodynamic Casimir effect, see Sec. IV of Ref. 30. In terms of eigenvalues λ_α and eigenvectors $|\alpha\rangle$ of the transfer matrix, the thermodynamic Casimir force per area can be written as

$$\frac{1}{k_B T} F_{\mathrm{Casimir}} = -\frac{1}{L^2} \frac{\sum_\alpha m_\alpha \exp(-m_\alpha l)\ \langle b_1|\alpha\rangle\langle b_2|\alpha\rangle}{\sum_\alpha \exp(-m_\alpha l)\ \langle b_1|\alpha\rangle\langle b_2|\alpha\rangle}, \tag{79}$$

where $1/\xi_\alpha = m_\alpha = -\ln(\lambda_\alpha/\lambda_0)$. Note that here m is a mass and should not be confused with the magnetization. We assume that the eigenvalues are ordered such that $\lambda_\alpha \geqslant \lambda_\beta$ for $\alpha < \beta$, where α, β are positive integers or zero. The states $|b_1\rangle$ and $|b_2\rangle$ are defined by the boundary conditions that are applied and $l = L_0 + 1$. For $x_t \gg 0$, the right side of Eq. (79) is dominated by the contribution from the state $|1\rangle$ and, therefore,

$$\tilde{\theta}_{(b_1,b_2)}(ml) \approx -m^3 l^3 \exp(-ml) C(b_1) C(b_2), \tag{80}$$

where we have identified $1/\xi = m = m_1$ and we have defined

$$C(b) = \frac{1}{mL} \frac{\langle b|1\rangle}{\langle b|0\rangle}. \tag{81}$$

The state $|0\rangle$ is symmetric under the global transformation $s_x \to -s_x$ for all x in a slice. Instead, $|1\rangle$ is antisymmetric and therefore $C = C(+) = -C(-)$. It follows that

$$\tilde{\theta}_{(+,+)}(ml) = -\tilde{\theta}_{(+,-)}(ml) = -C^2\, m^3 l^3 \exp(-ml) \tag{82}$$

for sufficiently large values of ml. Since $x_t = t[l/\xi_0]^{1/\nu} \simeq (ml)^{1/\nu}$, it follows that

$$\theta_{(+,+)}(x_t) = -\theta_{(+,-)}(x_t) = -C^2 x_t^{3\nu} \exp\left(-x_t^\nu\right) \tag{83}$$

for sufficiently large values of x_t. In the case of free boundary conditions, the boundary state $|0\rangle$ is symmetric under the global transformation $s_x \to -s_x$. Therefore, $\langle b|1\rangle$ vanishes and

$$C(0) = 0. \tag{84}$$

Next we have studied the first derivative of the scaling function with respect to h_1. In Fig. 6, we have plotted

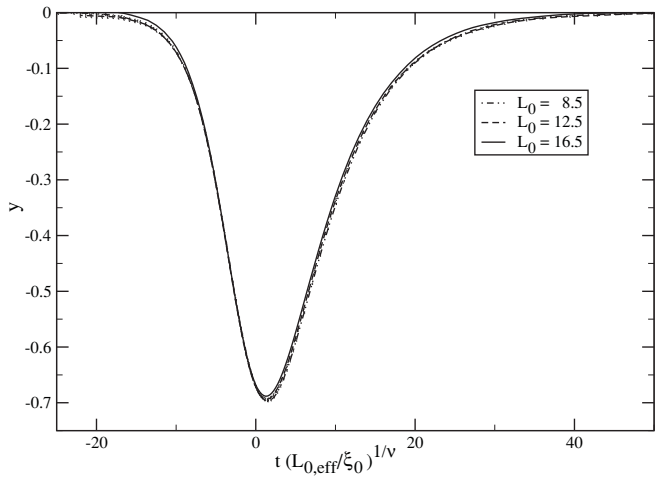

FIG. 6. We plot $y = -L_{0,\mathrm{eff}}^3 (L_{0,\mathrm{eff}}/l_{\mathrm{ex,nor},0})^{-y_{h_1}} \frac{\partial \Delta f_{\mathrm{ex}}}{\partial h_1}$ as a function of $t(L_{0,\mathrm{eff}}/\xi_0)^{1/\nu}$ for $(0,+)$ boundary conditions for the thicknesses $L_0 = 8.5$, 12.5, and 16.5. To this end, we have used $L_{0,\mathrm{eff}} = L_0 + L_s$ with $L_s = 1.43$, $\xi_0 = 0.2282$, and $\nu = 0.630\,02$.

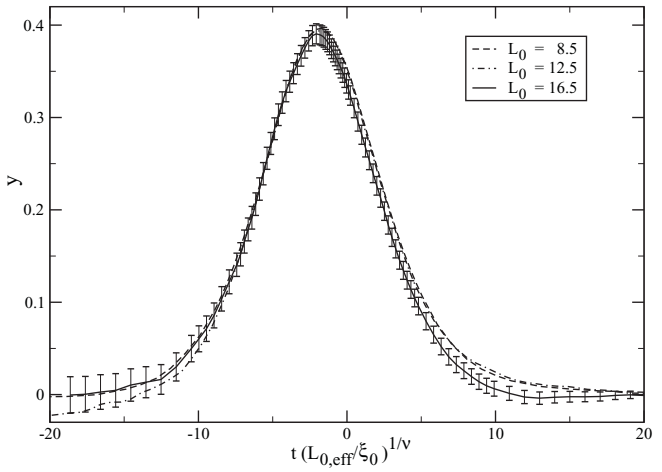

FIG. 7. We plot $y = -L_{0,\mathrm{eff}}^3 (L_{0,\mathrm{eff}}/l_{\mathrm{ex,nor},0})^{-2y_{h_1}} \frac{\partial^2 \Delta f_{\mathrm{ex}}}{\partial h_1^2}$ as a function of $t(L_{0,\mathrm{eff}}/\xi_0)^{1/\nu}$ for $(0,+)$ boundary conditions for the thicknesses $L_0 = 8.5$, 12.5, and 16.5. To this end, we have used $L_{0,\mathrm{eff}} = L_0 + L_s$ with $L_s = 1.43$, $\xi_0 = 0.2282$, and $\nu = 0.630\,02$.

$-L_{0,\mathrm{eff}}^3 (L_{0,\mathrm{eff}}/l_{\mathrm{ex,nor},0})^{-y_{h_1}} \frac{\partial \Delta f_{\mathrm{ex}}}{\partial h_1}$ as a function of $t(L_{0,\mathrm{eff}}/\xi_0)^{1/\nu}$. We do not give error bars, since the statistical error is of similar size to the thickness of the lines. We find that the data for $L_0 = 8.5$, 12.5, and 16.5 fall quite nicely on top of each other. The small discrepancies that are visible for large absolute values of x_t might be attributed to analytic corrections. We conclude that our numerical results provide a good approximation of the finite-size scaling function $\theta'(x_t) \equiv \frac{\partial \Theta(x_t,x_{h_1})}{\partial h_1}|_{h_1=0}$. We read off from Fig. 6 that θ' is negative throughout and has a single minimum.

We determined the location of this minimum by searching for the zero of $\frac{\partial \Delta E}{\partial h_1}$. We found $\beta_{\min} = 0.384\,03(3)$, $0.385\,77(2)$, and $0.386\,45(2)$ for $L_0 = 8.5$, 12.5, and 16.5, respectively. This corresponds to $x_{t,\min} = 1.473(18)$, 1.333(18), and 1.296(24). Here we have taken into account the errors of $\beta_{\min}$, L_s, and ν. In particular, for $L_0 = 16.5$, the error of $\beta_{\min}$ clearly dominates. The results for $L_0 = 12.5$ and 16.5 are consistent. As values of the derivative of the scaling function, we obtain $-0.697(13)$, $-0.696(14)$, and $-0.688(13)$ for $L_0 = 8.5$, 12.5, and 16.5, respectively. Note that in all cases, about half of the error is due to the uncertainty in $l_{\mathrm{ex,nor},0} = 0.213(3)$. The results for the different lattice sizes are consistent within the quoted errors. We conclude that

$$x_{t,\min} = 1.30(5), \quad \theta'_{\min} = -0.69(2). \tag{85}$$

Assuming that $C(h_1)$ is an analytic function and the finite-size scaling behavior (35) of the thermodynamic Casimir force per area, we arrive at

$$\theta'(x_t) = B x_t^{3\nu-\Delta_1} \exp\left(-x_t^{\nu}\right) \tag{86}$$

for $x_t \gg 0$. Matching our numerical data for $L_0 = 16.5$ at $x_t \approx 10$ with Eq. (86), we arrive at $B = -0.85(5)$, where the error is estimated by comparing with the result obtained from $L_0 = 12.5$.

Next, we studied the second derivative of the scaling function with respect to h_1. To this end, in Fig. 7 we have plotted $-L_{0,\mathrm{eff}}^3 (L_{0,\mathrm{eff}}/l_{\mathrm{ex,nor},0})^{-2y_{h_1}} \frac{\partial^2 \Delta f_{\mathrm{ex}}}{\partial h_1^2}$ as a function of $t(L_{0,\mathrm{eff}}/\xi_0)^{1/\nu}$. For $L_0 = 16.5$, we have plotted the statistical error, which we have not done for $L_0 = 8.5$ and 12.5 to keep the figure readable. Within our statistical accuracy, the curves for the three different thicknesses fall on top of each other. It seems that θ'' is positive for all values of the scaling function. Likely the negative values found for large $|x_t|$ and $L_0 = 16.5$ are just an artifact due to statistical fluctuations. The function displays a single maximum that is located at

$$x_{t,\min} = -1.9(2), \quad \theta''_{\min} = -0.39(2). \tag{87}$$

In Fig. 8, we have plotted $\theta_{(0,+)}$, $\theta'_{(0,+)}$, and $\theta''_{(0,+)}$. To this end, we have used the results obtained for $L_0 = 16.5$. We find that the shape of $\theta''_{(0,+)}$ is quite similar to that of $\theta_{(0,+)}$. In particular, for $x_t \to \infty$, both $\theta_{(0,+)}$ and $\theta''_{(0,+)}$ approach zero much faster than $\theta'_{(0,+)}$. Therefore, already for an infinitesimally small positive value of x_{h_1}, the crossover scaling function $\Theta(x_t,x_{h_1})$, taken as a function of x_t, has a minimum in the high-temperature phase.

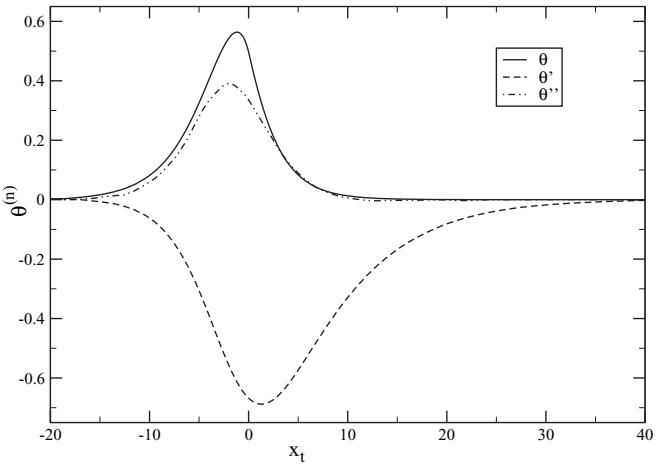

FIG. 8. We plot $\theta_{(0,+)}$, $\theta'_{(0,+)}$, and $\theta''_{(0,+)}$ as a function of x_t.

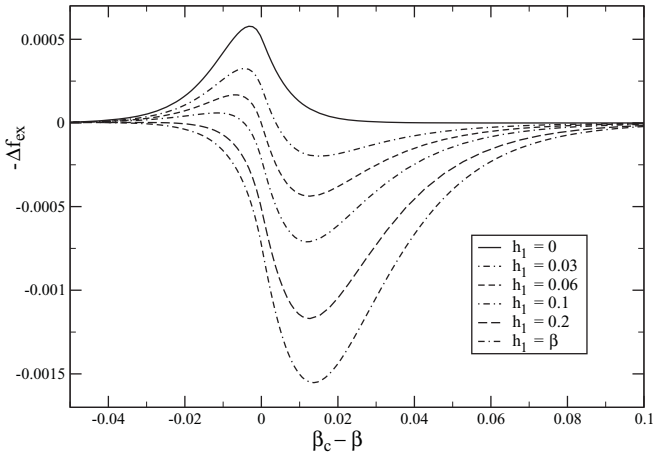

FIG. 9. We plot $-\Delta f_{ex}$ for $(h_1,+)$ boundary conditions as a function of the reduced temperature $\beta_c - \beta$. The thickness of the film is $L_0 = 8.5$ throughout.

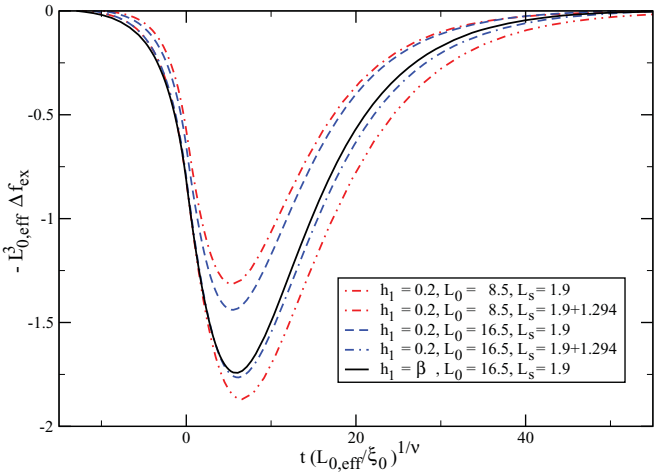

FIG. 10. (Color online) We plot $L_{0,\mathrm{eff}}^3 \Delta f_{ex}$ as a function of $t(L_{0,\mathrm{eff}}/\xi_0)^{1/\nu}$ for $h_1 = 0.2$ and $L_0 = 8.5$ and 16.5 using $L_s = 1.9$ or $L_s = 1.9 + 1.294$. For comparison, we give the corresponding curve for $L_0 = 16.5$ and $(+,+)$ boundary conditions using $L_s = 1.9$. For a discussion, see the text.

To check the range of applicability of the Taylor expansion, and to study the crossover beyond the Taylor expansion, we simulated films with $(h_1,+)$ boundary conditions and thicknesses $L_0 = 8$ and 9 at the values $h_1 = 0.03$, 0.06, 0.1, and 0.2 of the external field at the boundary. Our results along with that for $(+,+)$ corresponding to $h_1 = \beta$ obtained in Ref. 30 are plotted in Fig. 9. For $h_1 = 0.03$, there is a minimum of the thermodynamic Casimir force per area in the high-temperature phase. Its absolute value is about one-third of the value of the maximum in the low-temperature phase. The thermodynamic Casimir force changes sign at $\beta \approx 0.384$, which is slightly smaller than β_c. Going to larger values of h_1, the position of the minimum changes only little and the absolute value of the minimum increases. On the other hand, the value of the maximum is decreasing with increasing h_1. For $h_1 = 0.2$, the maximum has vanished.

The authors of Ref. 15 show in Fig. 9 of their paper Monte Carlo data obtained by Vasilyev[16] for the three-dimensional Ising model and the film thickness $L_0 = 10$. There is nice qualitative agreement with our results given in Fig. 9.

We have compared the results for the thermodynamic Casimir force per area obtained by simulating at $h_1 = 0.03$, 0.06, 0.1, and 0.2 for $L_0 = 8.5$ with those obtained by the Taylor expansion around $h_1 = 0$ up to second order in h_1. We found that for $h_1 = 0.03$, the results almost agree within the statistical error. Still for $h_1 = 0.06$, the Taylor expansion to second order resembles the true result quite well. The largest discrepancy is found for the value of the maximum of the thermodynamic Casimir force per area. It is overestimated by about a factor of 1.24. As one might expect, the result of the Taylor expansion becomes increasingly worse with increasing h_1. In particular, it does not reproduce that for large values of h_1 the maximum of the thermodynamic Casimir force per area disappears.

Given our results for various thicknesses L_0 at $h_1 = 0$, we conclude that the results for $L_0 = 8.5$ provide already a quite good approximation of the scaling limit. In particular, we are confident that the qualitative features of the crossover discussed here still hold in the scaling limit. In particular, we conclude that for $x_{h_1} \lessapprox 0.03[(8.5 + 1.43)/0.213]^{0.7249} \approx 0.5$, the scaling function $\Theta(x_t, x_{h_1})$ is still well described by the Taylor expansion around $x_{h_1} = 0$ to second order.

From Fig. 9, we can see that the thermodynamic Casimir force can also change sign as a function of the thickness L_0 for fixed values of h_1 and temperature. In general, both $x_t = t[L_0/\xi_0]^{y_t}$ and $x_{h_1} = h_1[L_0/l_{\mathrm{ex,nor},0}]^{y_{h_1}}$ depend on the thickness L_0. Therefore, for simplicity let us consider the bulk critical temperature, where $x_t = 0$ for any thickness of the film. For small L_0, the scaling variable x_{h_1} is small and therefore the thermodynamic Casimir force is close to the case $x_{h_1} = 0$ and is therefore repulsive. As L_0 increases, x_{h_1} increases and therefore $\Theta(0, x_{h_1})$ decreases. We see from Fig. 9 that $\Theta(0, x_{h_1}) \approx 0$ for $x_{h_1} \approx 1$. With further increasing L_0, the thermodynamic Casimir force becomes attractive.

1. *Approach to the $h_1 \to \infty$ limit*

For sufficiently large values of $x_{h_1} = h_1(L_0/l_{\mathrm{ex,nor},0})^{y_{h_1}}$, we expect that corrections to the $x_{h_1} \to \infty$ limit can be described by replacing L_0 by $L_{0,\mathrm{eff}} = L_0 + L_s$, where

$$L_s = l_{\mathrm{ex,nor}}(h_1) + l_{\mathrm{ex,nor}}(h_2). \tag{88}$$

In Fig. 10, we have plotted our results for $h_1 = 0.2$ and $L_0 = 8.5$ and 16.5. First, we use $L_s = 1.9$, which we had obtained in Ref. 30 for $(+,+)$ boundary conditions, and second, we use $L_s = 1.9 + 1.294$, where we have added $\Delta l_{\mathrm{ex,nor}}(0.2, \beta_c)$ obtained in Sec. VI B above. For comparison, we give the result obtained for $L_0 = 16.5$ and $(+,+)$ boundary conditions using $L_s = 1.9$. In the case of $L_0 = 8.5$, the matching with the $(+,+)$ result is somewhat improved by using $L_s = 1.9 + 1.294$ instead of $L_s = 1.9$. While the value of the minimum is clearly improved, the matching of the curve with that for $(+,+)$ boundary conditions deep in the high temperature phase is not. In contrast, for $L_0 = 16.5$, using $L_s = 1.9 + 1.294$ instead of $L_s = 1.9$ clearly improves the matching of the curve for

$h_1 = 0.2$ with that for $h_1 = \beta$ in the whole range of x_t that is considered.

We conclude that for $L_0 \gtrapprox 10\Delta l_{\mathrm{ex,nor}}(h_1,\beta_c)$, using $L_s = 1.9 + \Delta l_{\mathrm{ex,nor}}(h_1,\beta_c)$ clearly improves the matching with the $(+,+)$ scaling function. It would be desirable to check this by simulations for smaller values of h_1. However, this would be quite expensive, since already for $h_1 = 0.15$ we would need to simulate a thickness $L_0 \approx 30$.

VII. SUMMARY AND CONCLUSIONS

We have studied the crossover behaviors of a surface of a system in a three-dimensional Ising universality class from the ordinary to the normal or extraordinary surface universality class. To this end, we have simulated the improved Blume-Capel model on the simple cubic lattice. In particular, we have studied films with various boundary conditions applied. "Improved" means that corrections to finite-size scaling $\propto L_0^{-\omega}$ have a vanishing amplitude, where L_0 is the thickness of the film and $\omega = 0.832(6)$ (Ref. 36) is the exponent of leading corrections. This property is very useful in the study of films, since corrections $\propto L_0^{-1}$ due to the surfaces are expected,[54] and when fitting data it is difficult to disentangle corrections with similar exponents such as ω and 1. Mostly we have simulated films with $(0,+)$ boundary conditions. This means that at one surface we apply free boundary conditions, while at the other surface the spins are fixed to $+1$. Studying the magnetization of the slice at the surface with free boundary conditions, at the bulk critical point, of films of a thickness up to $L_0 = 64$, we arrive at the estimate $y_{h_1} = 0.7249(6)$ for the renormalization-group exponent of the external field at the surface for the ordinary surface universality class. This estimate is more accurate by at least a factor of 5 than those previously given in the literature. The authors of Ref. 51 quote an error that is only 2.5 times larger than ours, however the deviation between our estimate and theirs is about six times larger than the combined errors. For details, see Table I. We have studied the magnetization profile in the neighborhood of the surfaces for both the ordinary as well as the normal surface universality class. The data are consistent with the theoretically predicted power-law behavior. This study also allowed us to determine the extrapolation length l_{ex} for free boundary conditions as well as symmetry-breaking boundary conditions for various values of the external field h_1 at the surface. Corrections to scaling $\propto L_0^{-1}$, which are due to the surfaces of the film, can be expressed by an effective thickness $L_{0,\mathrm{eff}} = L_0 + L_s$, where L_s depends on the details of the model. Our numerical results confirm the hypothesis that $L_s = l_{\mathrm{ex},1} + l_{\mathrm{ex},2}$, where $l_{\mathrm{ex},1}$ and $l_{\mathrm{ex},2}$ are the extrapolation lengths at the two surfaces of the film.

Next, we studied the thermodynamic Casimir force in the neighborhood of the bulk critical point in the range of temperatures where it does not vanish at the level of our accuracy. First, we simulated films with $(0,+)$ boundary conditions and thicknesses $L_0 = 8.5$, 12.5, and 16.5. Taking into account corrections by replacing L_0 by $L_{0,\mathrm{eff}}$, the behavior of the thermodynamic Casimir force and its first and second derivative with respect to h_1 follows quite nicely the predictions of finite-size scaling. Hence our data allow us to compute good estimates of the finite-size scaling functions $\theta_{(0,+)}$, $\theta'_{(0,+)}$, and $\theta''_{(0,+)}$. Next we computed the thermodynamic Casimir force per area for the thickness $L_0 = 8.5$ at the finite values $h_1 = 0.03$, 0.06, 0.1, and 0.2 of the external field at the boundary. We find that the Taylor expansion of the thermodynamic Casimir force up to second order in h_1 around $h_1 = 0$ still describes the full function well at $h_1 = 0.03$, which corresponds to the value $x_{h_1} = h_1[L_0/l_{0,\mathrm{ex,nor}}]^{y_{h_1}} \approx 0.5$ of the scaling variable of the external field at the boundary. Finally, we studied the approach of the thermodynamic Casimir force to the limit $h_1 \to \infty$. We found that by using $L_{0,\mathrm{eff}} = L_0 + L_s(h_1)$, the corrections to this limit are well described for $L_0 \gtrapprox 10[L_s(h_1) - L_s(\beta_c)]$.

Based on exact results for stripes of the two-dimensional Ising model,[14] mean-field calculations,[15] and preliminary Monte Carlo results for the Ising model[16] on the simple cubic lattice, one expects that for certain combinations of the external fields h_1, h_2, and the thickness of the lattice L_0, the thermodynamic Casimir force changes sign as a function of the temperature. Also for certain choices of the external fields h_1, h_2, and the temperature, the thermodynamic Casimir force changes sign as a function of the thickness of the film. Here we confirm these qualitative findings.

ACKNOWLEDGMENTS

This work was supported by the DFG under Grant No. HA 3150/2-1.

*Martin.Hasenbusch@physik.hu-berlin.de

[1] M. E. Fisher and P.-G. de Gennes, C.R. Seances Acad. Sci. Ser. B **287**, 207 (1978).
[2] H. B. G. Casimir, Proc. K. Ned. Akad. Wet. **51**, 793 (1948).
[3] A. Gambassi, J. Phys.: Conf. Ser. **161**, 012037 (2009).
[4] M. N. Barber, *Finite-size Scaling*, in *Phase Transitions and Critical Phenomena*, edited by C. Domb and J. L. Lebowitz (Academic, London, 1983), Vol. 8.
[5] M. Krech, *The Casimir Effect in Critical Systems* (World Scientific, Singapore, 1994).
[6] K. G. Wilson and J. Kogut, Phys. Rep. C **12**, 75 (1974).
[7] M. E. Fisher, Rev. Mod. Phys. **46**, 597 (1974).
[8] M. E. Fisher, Rev. Mod. Phys. **70**, 653 (1998).
[9] A. Pelissetto and E. Vicari, Phys. Rep. **368**, 549 (2002).
[10] K. Binder, *Critical Behaviour at Surfaces*, in *Phase Transitions and Critical Phenomena*, edited by C. Domb and J. L. Lebowitz (Academic, London, 1983), Vol. 8.
[11] H. W. Diehl, *Field-theoretical Approach to Critical Behaviour at Surfaces*, in *Phase Transitions and Critical Phenomena*, edited by C. Domb and J. L. Lebowitz (Academic, London, 1986), Vol. 10, p. 76.
[12] H. W. Diehl, Int. J. Mod. Phys. B **11**, 3503 (1997).
[13] F. M. Schmidt and H. W. Diehl, Phys. Rev. Lett. **101**, 100601 (2008).

[14]D. B. Abraham and A. Maciołek, Phys. Rev. Lett. **105**, 055701 (2010).
[15]T. F. Mohry, A. Maciołek, and S. Dietrich, Phys. Rev. E **81**, 061117 (2010).
[16]O. Vasilyev, private communication to the authors of Ref. 15. Further preliminary results were presented as a poster at the Workshop "Fluctuation Induced Forces in Condensed Matter," Dresden, 2010 [http://www.mpipks-dresden.mpg.de/∼fifcm10/].
[17]P. Ball, Nature (London) **447**, 772 (2007).
[18]U. Nellen, L. Helden, and C. Bechinger, Europhys. Lett. **88**, 26001 (2009).
[19]M. Tröndle, S. Kondrat, A. Gambassi, L. Harnau, and S. Dietrich, Europhys. Lett. **88**, 40004 (2009).
[20]M. Tröndle, S. Kondrat, A. Gambassi, L. Harnau, and S. Dietrich, J. Chem. Phys. **133**, 074702 (2010).
[21]A. Gambassi and S. Dietrich, Soft Matter **7**, 1247 (2011).
[22]M. Tröndle, O. Zvyagolskaya, A. Gambassi, D. Vogt, L. Harnau, C. Bechinger, and S. Dietrich, e-print arXiv:1012.0181.
[23]B. V. Derjaguin, Kolloid Z. **69**, 155 (1934).
[24]A. Hanke, F. Schlesener, E. Eisenriegler, and S. Dietrich, Phys. Rev. Lett. **81**, 1885 (1998).
[25]F. Schlesener, A. Hanke, and S. Dietrich, J. Stat. Phys. **110**, 981 (2003).
[26]C. Hertlein, L. Helden, A. Gambassi, S. Dietrich, and C. Bechinger, Nature (London) **451**, 172 (2008).
[27]A. Gambassi, A. Maciołek, C. Hertlein, U. Nellen, L. Helden, C. Bechinger, and S. Dietrich, Phys. Rev. E **80**, 061143 (2009).
[28]O. Vasilyev, A. Gambassi, A. Maciołek, and S. Dietrich, Europhys. Lett. **80**, 60009 (2007).
[29]O. Vasilyev, A. Gambassi, A. Maciołek, and S. Dietrich, Phys. Rev. E **79**, 041142 (2009).
[30]M. Hasenbusch, Phys. Rev. B **82**, 104425 (2010).
[31]A. Hucht, Phys. Rev. Lett. **99**, 185301 (2007).
[32]M. Krech and D. P. Landau, Phys. Rev. E **53**, 4414 (1996).
[33]M. Hasenbusch, Phys. Rev. E **80**, 061120 (2009).
[34]D. Dantchev and M. Krech, Phys. Rev. E **69**, 046119 (2004) .
[35]Y. Deng and H. W. J. Blöte, Phys. Rev. E **70**, 046111 (2004).
[36]M. Hasenbusch, Phys. Rev. B **82**, 174433 (2010).
[37]M. Hasenbusch, Phys. Rev. B **82**, 174434 (2010).
[38]C. J. Silva, A. A. Caparica, and J. A. Plascak, Phys. Rev. E **73**, 036702 (2006).
[39]T. W. Burkhardt and H. W. Diehl, Phys. Rev. B **50**, 3894 (1994).
[40]T. W. Burkhardt and E. Eisenriegler, Phys. Rev. B **16**, 3213 (1977); **17**, 318 (1978).
[41]S. G. Whittington, G. M. Torrie, and A. J. Guttmann, J. Phys. A **19**, 2449 (1979).
[42]H. W. Diehl and S. Dietrich, Z. Phys. B **42**, 65 (1981).
[43]H. W. Diehl and M. Shpot, Nucl. Phys. B **528**, 595 (1998).
[44]K. Binder and D. P. Landau, Phys. Rev. Lett. **52**, 318 (1984).
[45]M. Kikuchi and Y. Okabe, Prog. Theor. Phys. **73**, 32 (1985).
[46]D. P. Landau and K. Binder, Phys. Rev. B **41**, 4633 (1990).
[47]M. P. Nightingale and H. W. J. Blöte, Phys. Rev. B **48**, 13678 (1993).
[48]C. Ruge and F. Wagner, Phys. Rev. B **52**, 4209 (1995).
[49]M. Pleimling and W. Selke, Eur. Phys. J. B **1**, 385 (1998) .
[50]Y. Deng and H. W. J. Blöte, Phys. Rev. E **67**, 066116 (2003).
[51]Y. Deng, H. W. J. Blöte, and M. P. Nightingale, Phys. Rev. E **72**, 016128 (2005).
[52]S. Z. Lin and B. Zheng, Phys. Rev. E **78**, 011127 (2008).
[53]M. Smock, H. W. Diehl, and D. P. Landau, Ber. Bunsenges. Phys. Chem. **98**, 486 (1994).
[54]H. W. Diehl, S. Dietrich, and E. Eisenriegler, Phys. Rev. B **27**, 2937 (1983).
[55]S. Leibler and L. Peliti, J. Phys. C **15**, L403 (1982); E. Brézin and S. Leibler, Phys. Rev. B **27**, 594 (1983).
[56]T. W. Capehart and M. E. Fisher, Phys. Rev. B **13**, 5021 (1976).
[57]R. C. Brower and P. Tamayo, Phys. Rev. Lett. **62**, 1087 (1989).
[58]R. H. Swendsen and J.-S. Wang, Phys. Rev. Lett. **58**, 86 (1987).
[59]U. Wolff, Phys. Rev. Lett. **62**, 361 (1989).
[60]M. Saito and M. Matsumoto, *SIMD-oriented Fast Mersenne Twister: A 128-bit Pseudorandom Number Generator*, in *Monte Carlo and Quasi-Monte Carlo Methods 2006*, edited by A. Keller, S. Heinrich, and H. Niederreiter (Springer, Berlin, Heidelberg, 2008); M. Saito, Master's thesis, Hiroshima University (2007). The source code of the program is provided at [http://www.math.sci.hiroshima-u.ac.jp/∼m-mat/MT/SFMT/index.html].
[61]M. Krech, Phys. Rev. E **56**, 1642 (1997).
[62]J. L. Cardy, Nucl. Phys. B **275**, 200 (1986).